

ISSN 2095-9273  
CN 10-1298/N

# Science Bulletin

Volume 60 · Number 22 · November 2015



**In this issue:**

***Mantle-derived magmas:  
intraplate, hot-spots and mid-ocean ridges***  
**(David H. Green & Trevor J. Falloon, P. 1873-1900)**

 SCIENCE CHINA PRESS

 Springer

Chinese Academy of Sciences  
National Natural Science Foundation of China



## Experimental demonstrations on the sources and conditions of mantle melting

Yaoling Niu

Published online: 4 November 2015

© Science China Press and Springer-Verlag Berlin Heidelberg 2015

The Earth's chemical differentiation is largely the result of mantle melting and magma evolution. Our present-day knowledge of mantle melting and magma evolution owes much to experimental simulations carried out by a handful of experimental petrologists over the last ~50 years. Professor David Green is one of these few pioneers, whose contributions are enormous and fundamental, and have laid the foundations for our current understanding of mantle melting at ocean ridges, above subduction zones and in intraplate settings on land and in the oceans. In this issue, Professor Green summarizes the state-of-the-art understanding on the sources and conditions of mantle melting from the perspectives of experimental petrology [1]. David received both BSc (1957) and MSc (1960) degrees in geology from the University of Tasmania, and a PhD (1962) in Mineralogy and Petrology from the University of Cambridge. From 1962 to 1976, David joined the Australian National University (ANU) as Research Fellow, Senior Fellow and Professorial Fellow, carrying out many of the cornerstone experimental studies. From 1977 to 1994, David was Professor of Geology at the University of Tasmania, continuing his research while also serving as Chief Science Adviser in the Commonwealth Department of Arts, Sport, the Environment and Territories in Canberra (1991–1993). From 1994 to 2001, David served as the Director of the Research School of Earth Sciences at the ANU (Deputy Vice-Chancellor in 1998). He retired in 2001 as Professor Emeritus at the ANU and at the University of Tasmania since 2008, continuing to publish innovative research results. Professor Green has published

over 220 research papers with huge impact as manifested by over 24,000 citations with an h-index of 82 (as of 15 October 2015 in Google Scholar).

Professor Green's research, together with his graduate students, post-doctoral fellows and colleagues, has revealed the complexity of the Earth's upper mantle and deep crust and provided experimentally calibrated phase equilibria that have facilitated the interpretations of geological and geophysical observations on varying scales in a global context. His earlier work focused on the phase-relations and melting behaviour of mantle peridotite to form the basaltic ocean crust and on the high pressure reactions to produce eclogite and garnet peridotite. This work pioneered the application of electron probe micro-analysis to experimentally produced mineral assemblages, including high pressure melt compositions. The systematic determination of melt compositions in model mantle compositions as functions of pressure and temperature led to models for genesis of mid-ocean ridge basalts, island-chain or "hot-spot" basalts and intraplate basalts ranging from kimberlites to basanites and alkali basalts. The experimental study of gabbro to eclogite transformation led to calibration of the garnet/clinopyroxene geothermometer and to studies of other rock compositions at deep crust to upper mantle conditions. With the discovery of quench-textured, extremely olivine-rich peridotitic komatiites in the earliest Archaean terranes, David combined the experimental determination of liquidus olivine and temperature with the analyses of the natural quenched olivine to demonstrate that they were extremely high temperature peridotitic melts, apparently restricted to the early Earth.

Professor Green and his co-workers, including his co-author on this paper, Dr. Trevor Falloon, have also demonstrated the fundamental roles of carbon and hydrogen (as water, methane, diamond or graphite, and carbon

Y. Niu (✉)

Department of Earth Sciences, Durham University,  
Durham DH1 3LE, UK  
e-mail: yaoling.niu@durham.ac.uk

dioxide) in the mineralogy and melting characteristics of the Earth. He has shown the importance of the hydrous mineral pargasite in storing water in the uppermost mantle and the sharp decrease in melting temperature with increasing pressure at about 90 km depth, due to the higher pressure instability of pargasite. This work has identified the petrological control on the “thin plate” behaviour of the Earth, known as “plate tectonics”. His petrological work, using both experiments and natural rocks, provides an effective explanation for the change in rheological, seismological and electrical properties at the lithosphere/asthenosphere boundary. He has documented the composition of the very small fraction (<1 %) of intergranular melt present in the asthenosphere as hydrous, carbonate-bearing silicate melts. These near-solidus melts are highly enriched in volatiles and incompatible elements and with their mobility can refertilize the asthenosphere and lithosphere, commonly known as “mantle metasomatism”. Such processes, in particular in the complex crust/mantle interactions at convergent plate boundaries, are fundamental to understanding the mantle chemical and isotopic heterogeneity in the deep Earth.

Professor Green’s group has also used experimental methods to calibrate a mineral-based sensor for oxygen fugacity (Fe–Al–Cr spinel in peridotite) and applied this calibration to quantify different redox characteristics in different mantle settings. This led to studies of melting behaviour at different oxygen fugacities and to very specific models of melting and phase assemblages in the whole plate tectonic cycle from upwelling of lower asthenosphere to subduction of oxidized crust and lithosphere, and to their melting for intraplate magmatism with heterogeneous compositions.

In addition, as an investigator of lunar samples returned by the Apollo missions, Professor Green identified parental melt compositions in Apollo 12, 15 and 17 mare basalt samples and used experimental methods to constrain their conditions of genesis and implications for the Moon’s interior. Green’s laboratory has also documented the high-pressure mineralogy of diverse crustal compositions including basaltic, andesitic, pelitic and granitic and developed geothermometers and geobarometers among the most widely used and referenced tools in metamorphic petrology, including mapping the paths of crustal rocks subjected to deep burial, heating and upwelling.

David’s important scientific contributions have been recognized by numerous honours and awards, including the fellowships of Australian Academy of Science (1974), European Union of Geosciences (1985), Geological Society of America (1986), The Royal Society of London (1991), the Russian Academy of Sciences (2003) and American Geophysical Union (2004) as well as the Inaugural Jaeger Medal of Australian Academy of Science (1990), Werner Medal of the German mineralogical Society (1998), Murchison Medal of the Geological Society of London (2000), International Gold Medal of the Geological Society of Japan (2007) and the International Mineralogy Association Medal (2012). David was honoured as the Inaugural Shen-Su Sun Memorial Lecturer (2012), and gave the lecture *Mantle-derived magmas at mid-ocean ridges, hot-spots, and intraplate locations: Are hot-spots really hot and do deep-seated mantle plumes exist?* at the Annual National Petrology and Geodynamics Conference of China on 22 September 2012 in Lanzhou.

I am delighted that Professor Green accepted the invitation to contribute his lecture in this written and much more comprehensive form to *Science Bulletin*. In addition to the elegant reviews on fundamental principles and basic concepts that benefit us all in using petrology and geochemistry as means to interpreting Earth processes, David and his colleague, Dr. Trevor Falloon, demonstrates convincingly that despite the compositional differences between mid-ocean ridge basalts (MORB) and “hot-spot” magmas or ocean island basalts (OIB), there is no evidence that OIB mantle source is any hotter than MORB mantle source, and that there is no evidence to support the “deep mantle thermal plume” hypothesis. While it remains in debate whether mantle plumes exist or not, the key message here is that we must think objectively and analytically in order to genuinely understand the working of the Earth rather than passively follow bandwagons. This is particularly important for younger generations of Chinese Earth scientists.

## Reference

1. Green DH, Falloon TJ (2015) Mantle-derived magmas: intraplate, hot-spots and mid-ocean ridges. *Sci Bull* 60:1873–1900



# Mantle-derived magmas: intraplate, hot-spots and mid-ocean ridges

David H. Green · Trevor J. Falloon

Received: 25 August 2015 / Accepted: 25 September 2015 / Published online: 27 October 2015  
© Science China Press and Springer-Verlag Berlin Heidelberg 2015

**Abstract** Primary or parental magmas act as probes to infer eruption and source temperatures for both mid-ocean ridge (MOR) and ‘hot-spot’ magmas (tholeiitic picrites). The experimental petrogenetic constraints (‘inverse’ experiments) argue for no significant temperature differences between them. However, there are differences in major, minor and trace elements which characterise geochemical, not thermal, anomalies beneath ‘hot-spots’. We suggest that diapiric upwelling from interfaces (redox contrasts) between old subducted slab and normal MOR basalt source mantle is the major reason for the observed characteristics of island chain or ‘hot-spot’ volcanism. Intraplate basalts also include widely distributed volcanic centres containing lherzolite xenoliths, i.e. mantle-derived magmas. Inverse experiments on olivine basalt, alkali olivine basalt, olivine basanite, olivine nephelinite, olivine melilitite and olivine leucitite (lamproite) determined liquidus phases as a function of pressure, initially under anhydrous and CO<sub>2</sub>-absent conditions. Under C- and H-absent conditions, only tholeiites to alkali olivine basalts had Ol + Opx ± Cpx as high-pressure liquidus phases. Addition of H<sub>2</sub>O accessed olivine basanites at 2.5–3 GPa, ~1,200 °C, but both CO<sub>2</sub> and H<sub>2</sub>O were necessary to obtain saturation with Ol, Opx, Cpx and Ga at 2.5–3.5 GPa for olivine nephelinite and olivine melilitite. The forward and inverse experimental studies are combined to formulate a petrogenetic grid for intraplate, ‘hot-spot’ and MOR magmatism within the plate tectonics paradigm. The asthenosphere is geochemically zoned by slow upward migration of incipient melt. The solidus and phase

stabilities of lherzolite with very small water contents (<3,000 ppm) determine the thin plate behaviour of the oceanic lithosphere and thus the Earth’s convection in the form of plate tectonics. There is no evidence from the parental magmas of MOR and ‘hot-spots’ to support the ‘deep mantle thermal plume’ hypothesis. The preferred alternative is the presence of old subducted slabs, relatively buoyant and oxidised with respect to MORB source mantle and suspended or upwelling in or below the lower asthenosphere (and thus detached from overlying plate movement).

**Keywords** Mantle-derived magmas · High-pressure experiments · C–H–O · Asthenosphere · Hot-spots · Plate tectonics

## 1 Introduction

In the plate tectonics paradigm for the modern Earth, it is generally accepted that the primary differentiation of Earth’s crust from the upper mantle is the result of intrusion and extrusion of basalts at mid-ocean ridges, augmented by other intraplate basaltic volcanism at rift and ‘hot-spot’ (island chain) locations. A third process of crust formation by magmatism at convergent margins (subduction zones) involves both mantle and crustal components and is addressed only briefly in this paper. Closer examination of basaltic volcanism at mid-ocean ridges and intraplate locations reveals that basaltic volcanism is remarkably diverse in these settings. Some of this diversity is due to partial crystallisation, fractionation and mixing of magmas at shallow depths. A first step in understanding the mantle processes which cause basaltic volcanism is to

D. H. Green (✉) · T. J. Falloon  
Earth Sciences, School of Physical Sciences, University of Tasmania, Private Bag 79, Hobart, TAS 7001, Australia  
e-mail: david.h.green@utas.edu.au

direct attention to those magmas which have acquired their observed compositions by high-pressure processes, particularly in the partial melting and melt segregation from upper mantle peridotite. The central theme of this paper is the use of high-pressure and high-temperature experimental techniques to replicate upper mantle conditions and to determine the effects of pressure, temperature and compositional parameters on the compositions of melts and residues for model upper mantle compositions. This has been the traditional approach using both simple systems of few chemical components and complex, multi-component natural rock compositions. The latter approach has developed with the availability of microbeam techniques, particularly the electron microprobe, to document mineral and melt compositions.

The experimental approach to magma genesis uses major element compositions of models for the upper mantle. Experiments explore subsolidus mineralogy as a function of pressure ( $P$ ), temperature ( $T$ ) and activities of volatile components, particularly of C, H and O. Experiments also explore the initiation of melting (solidus) and melt/residue equilibrium with increasing melt fraction ('forward' experiments). Conversely, observed magma compositions proposed as primary or parental magmas are investigated to determine their liquidus phases as functions of  $P$ ,  $T$  and volatile components ('inverse' experiments) and also their crystallisation paths to yield derivative melts and possible cumulate rocks. In natural rocks, almost all minerals are solid solutions of several chemical components so that in addition to phase relations, the partitioning of components between melt and residual minerals provides important constraints on magma genesis.

From both theory and experiment, we know that melt compositions from a multiphase source such as lherzolite [olivine (Ol) > orthopyroxene (Opx) > clinopyroxene (Cpx) > plagioclase (Pl) or Al-rich spinel (Sp) or garnet (Ga)] are produced by a combination of both eutectic style and solid solution style melting. In simple eutectic melting, the composition of a melt at the solidus is fixed irrespective of the proportions of the subsolidus phases, but the amount of melt and proportions of residual phases vary with bulk composition. A calculated residue/melt partition coefficient for a particular component will vary with bulk (residue) composition. Depending on melt composition and bulk composition, one phase will disappear at the solidus. With increasing temperature, melt compositions are controlled by cotectic behaviour, and melts maintain saturation with remaining phases which are sequentially eliminated as melt fraction increases. Melt compositions are controlled by phase relationships, and the concept of a partition coefficient expressing residue/melt relationship only applies to a particular composition,  $P$  and  $T$  (an empirical value determined by experiment [1]).

In solid solution style melting of a single phase, the melt composition and solidus temperature are controlled by the subsolidus composition (i.e. by a mineral/melt partition coefficient), and the melt fraction is vanishingly small at the solidus and increases continuously with increasing temperature. With respect to particular solid solutions such as Fe–Mg or Na–Ca substitutions, partition coefficients for mineral/melt pairs may be functions of  $P$  and  $T$  only and thus constrain the melt composition. However, in multi-phase systems the bulk residue/melt partition will vary with residual mineralogy (bulk composition).

Major element compositions of mantle-derived magmas are defined by phase equilibria coupled with mineral/melt partition coefficients expressing the major solid solutions in residual minerals. For minor and trace elements, the use of partition coefficients is important. Minor and trace elements may be designated as 'compatible' if they have significant solid solution ( $D = c_{\text{mineral}}/c_{\text{melt}} > 0.1$ ;  $c$  = concentration) in the major phases (olivine, orthopyroxene, clinopyroxene, plagioclase, spinel or garnet) or 'incompatible' if  $c_{\text{mineral}}/c_{\text{melt}} < 0.1$ . Among the minor elements present in natural basalts and peridotites, K, P, H, C and S are highly incompatible with respect to lherzolite mineralogy. These elements are extremely important in magma genesis as they form additional phases (phlogopite, apatite, pargasite, graphite, carbonate, sulphide) even at low concentrations in the mantle and thus introduce new controls on the mantle solidus. In particular, H and C have major effects on solidus temperatures and through redox reactions (C, H, O fluids) have variable solubilities in melts. They may occur either as vapour (or super-critical fluid) phase ( $\text{H}_2$ ,  $\text{H}_2\text{O}$ ,  $\text{CH}_4$ ,  $\text{CO}_2$ ), as stoichiometric components in hydrous silicates (amphibole, mica), in minor or trace minerals (diamond or graphite, carbonates, apatite), or dissolved in silicate or carbonatite melts. There is current debate on the role of water in defect sites in nominally anhydrous minerals (NAMs—Ol, Opx, Cpx, Ga) in the upper mantle.

Within the plate tectonics paradigm, the basaltic magmatism at mid-ocean ridges (MORB) is recognised as sampling 'modern well-mixed mantle' or 'asthenospheric mantle' in the upwelling processes that create new basaltic crust + lithospheric mantle. In addition, a distinctive type of within-plate volcanism forms island chains (on oceanic crust) or volcanic lineaments (on continental crust) and implies movement of the lithospheric plate over a relatively 'fixed' but discontinuous magmatic source. This basaltic magmatism, exemplified by the Hawaiian volcanic chain, is commonly called 'hot-spot' volcanism and attributed to deep mantle plumes of hot, geochemically distinctive material arising from the core/mantle boundary (CMB) [2, 3]. These interpretations attribute 'hot-spot' magmatism to a different convection system from that expressed by the

lithospheric plates, mid-ocean ridges, transform faults and trenches, volcanic arcs and back-arc basins of plate tectonics. Also within plates, basaltic volcanism is observed accompanying lithospheric stretching associated with continental rifts, with lithospheric bending adjacent to oceanic trenches ('petit spot' volcanism [4]) and as isolated seamounts and islands, possibly linked to transform faults. The term 'intraplate basalts' (IB) or ocean island basalts (OIB) is used for this group or subsets within it.

This paper reviews the experimental approach, particularly the 'inverse' method, to understanding the origins of mantle-derived magmas. We particularly emphasise the distinctions between parental MORB and parental 'hot-spot' magmas. The roles and causes of 'hot-spots' within the plate tectonics hypothesis are controversial, and geophysical, geochemical and numerical modelling approaches are relevant [5]. The experimental approach directly tests a central postulate of the 'deep mantle plume' hypothesis, i.e. there is a temperature contrast ( $dT_p = 200\text{--}250\text{ }^\circ\text{C}$ ) between ambient mantle (MORB source) and upwelling 'plume' (hot-spot magma source) (where  $T_p$  is 'potential temperature' as used by McKenzie and Bickle [6]). The temperature difference provides buoyancy to the plume and is expressed in differences between the respective parental magmas [7]. We summarise experimental studies of parental MORB and 'hot-spot' magmas and integrate them with experimental studies of other mantle-derived intraplate magmas and also with the constraints from peridotite melting studies.

## 2 Parental magmas at mid-ocean ridges and 'hot-spots'

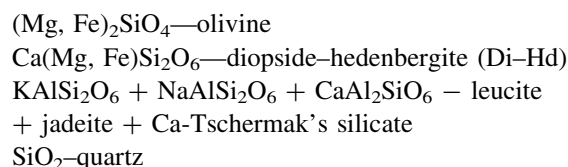
In the mid-twentieth century, the basaltic volcanoes of Hawaii had been well studied in terms of petrology, geochemistry, volcanology and geophysical monitoring. Studies of other volcanic provinces commonly were 'benchmarked' against the Hawaiian observations, particularly the tholeiitic basalts of the main cone-building phase. From the earliest sampling of the deep sea floor and mid-ocean ridge locations, it was recognised that there were strong similarities but also significant petrological differences between mid-ocean ridge and Hawaiian basalts, particularly if attention was drawn to the most magnesian glasses or aphyric rocks [higher Mg# where  $\text{Mg\#} = 100 \text{Mg}/(\text{Mg} + \text{Fe}^{2+})$ ]. Both groups are olivine tholeiites, transitional to picrites, i.e. they are olivine and hypersthene normative, and Mg# of olivine phenocrysts ranges up to  $\text{Mg}_{91}$  in both 'hot-spot' and MOR olivine tholeiites. Olivine and spinel are liquidus phases, but spinel in MORB is Al rich [ $\text{Cr\#} = 20\text{--}50$  where  $\text{Cr\#} = 100 \text{Cr}/(\text{Cr} + \text{Al})$ ] and is Cr rich in Hawaiian tholeiites ( $\text{Cr\#} = 60\text{--}70$ ). Clinopyroxene (Cpx) is the next phase to

crystallise in most Hawaiian tholeiite suites. However, in MORB, plagioclase crystallisation precedes clinopyroxene, and this reflects a significant difference in major element composition between the two groups and led to the original naming of MORB as 'high-alumina tholeiites' [8]. This difference in major element compositions in parental or primary compositions implies differences in phase relationships at source, i.e. either different source compositions or different conditions of melting and melt segregation from residual mantle (or both). Later work has established differences in minor and trace elements and in isotopic ratios, confirming heterogeneity in the source compositions. To explore the relative roles of source compositions and conditions of partial melting, the nature and compositions of liquidus phases of primary magmas must be established and matched to the melting behaviour of upper mantle peridotite. In the following section, we summarise experimental studies on melting of peridotite, emphasising the roles of water and carbon in lowering melting temperatures and diversifying the variety of primary melts from the mantle.

### 2.1 Primary magmas and constraints

from experimental studies of melting of peridotite

In sampling MORB and IB, the use of glass rather than bulk rock compositions selects melt compositions which may range from primary, mantle-derived melts to evolved melt compositions lying on crystallisation paths or low-pressure reaction paths controlled by low-pressure cotectics. The latter processes occur in magma chambers, magma channels, reactive porous flow, or impregnation and refertilisation in mantle/crust transition zones beneath mid-ocean ridges and central volcanoes. Recognising that olivine, clinopyroxene, orthopyroxene and spinel are known to be the phases present in these processes and are Mg–Fe solid solutions, we select the most magnesian glasses as 'parental'. To illustrate the compositional differences and similarities, the melt compositions are expressed in terms of end-member mineral compositions ('norms') rather than elements, oxides or oxide ratios. The chosen minerals are derived from those dominating low-pressure crystallisation (i.e. the CIPW norm) and are expressed as molecular proportions rather than weight proportions:



This method of comparison, using tetrahedral projections of the molecular normative components as listed, is

effective in capturing >95 % of the chemical variation of basaltic and peridotitic rocks and is useful in illustrating compositions in terms of phase relations. The fields of silica-oversaturated (quartz-normative), saturated (olivine and hypersthene normative) and silica-undersaturated (nepheline normative) magmas are identified, although extremely undersaturated magmas such as olivine nephelinites or olivine melilitites lie outside the tetrahedron ('basalt tetrahedron'). In addition to the normative projections, the importance of solid solutions in residue/melt relations is recognised by the use of Mg# [100 Mg/(Mg + Fe)] expressing the major solid solutions in pyroxenes and olivine, in which partitioning is such that melts are always more Fe rich than coexisting olivine or pyroxene(s).

Experimental studies of model mantle compositions at high pressures have established systematic compositional changes in melts as functions of melt fraction and pressure. These systematic melting trends for two model mantle compositions, designated MOR pyrolite (MPY) and

Hawaiian pyrolite (HPY), respectively, are plotted in the normative projections of Fig. 1 a–c. These experiments were carried out without H<sub>2</sub>O or CO<sub>2</sub> present. The diagrams illustrate the phase equilibria control of melt compositions, including the roles of pressure and of bulk composition. Thus, at low pressure (1 GPa) near-solidus melts are in equilibrium with residual plagioclase lherzolite. With increasing temperature, the melt fraction increases and liquidus phases sequentially eliminated to finally reach a dunite [Ol + Sp(Cr)] cotectic. In addition, each mineral shows systematic compositional changes reflecting partition relations between mineral and melt. Particularly, useful relations are Mg/Fe in olivine, Cr/Al in spinel and Ca/Na in plagioclase and clinopyroxene. Figure 1 (the 'basalt tetrahedron') thus shows a template against which particular melt compositions can be evaluated as possible primary melts from a source lherzolite at various pressures and melt fractions. In addition to the use of the 'basalt tetrahedron', the compositions of liquidus phases of the possible primary melt at the *P*, *T* of interest

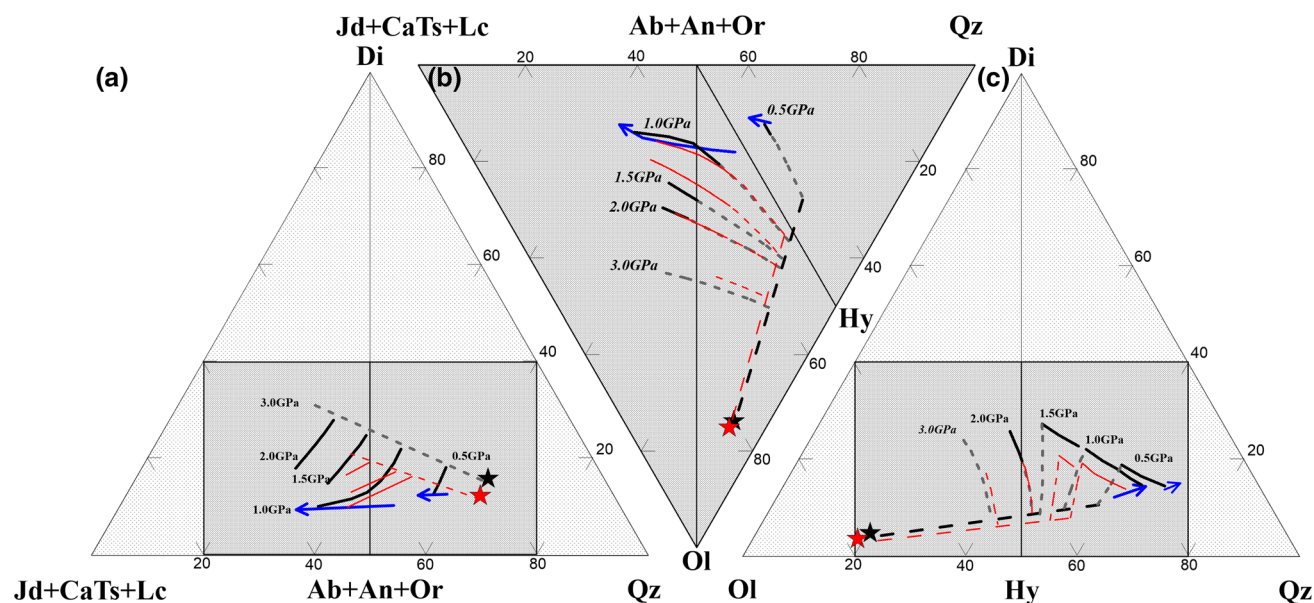


**Fig. 1** (Color online) The normative-based 'basalt tetrahedron' is used to illustrate the primacy of phase equilibria in determining the compositions of melts in lherzolite at increasing pressure and in the absence of (C, H, O) volatiles. The compositions of melts were determined by experimental studies of 'fertile' (MPY—red star) and 'enriched' (HPY—black star) lherzolite compositions at increasing temperature and melt fraction and pressures from 0.5 to 3 GPa. The melt compositions at or near the solidi lie on six-phase cotectics (blue arrows) at low pressure (Ol + Opx + Cpx + Plag + Cr spinel + melt) and five-phase cotectics (red and black solid lines) at 1.5–3 GPa (Ol + Opx + Cpx + Cr–Al spinel + melt). As temperature increases at each pressure, melt fraction increases and residual phases dissolve sequentially, i.e. plagioclase followed by clinopyroxene and then orthopyroxene at low pressure; clinopyroxene followed by orthopyroxene at intermediate pressure and garnet followed by clinopyroxene at 3–3.5 GPa. Spinel increases in Cr# [100 Cr/(Cr + Al)] with increasing melt fraction at all pressures. Harzburgite [Ol + Opx + Cr spinel (red and grey short-dashed lines)] to dunite [Ol + chromite (red and black long dashed lines)] are the residue for greater than ~30 % melting at all pressures to 4 GPa. Particular minerals show changes in solid solution of refractory, compatible and mildly incompatible elements (Cr, Al, Ca, Fe, Ti, Na) as functions of melt fraction and pressure. The 'basalt tetrahedron' captures >95 % of the compositional variation in peridotite and basalts, and normative projections illustrate phase equilibria controls more clearly than oxide or oxide ratio plots (e.g. use of terms such as 'high-alumina basalts', 'high-Fe basalts', 'calc-alkali basalts', 'alkali basalts'). **a** Projection from olivine (Ol), **b** projection from diopside (Di), **c** projection from jadeite + calcium tschermakite + leucite (Jd + CaTs + Lc). This figure is derived from data in [18, 72]

should closely match those of the residual phases in the model lherzolite. It is possible to use a variety of projections within the tetrahedron to illustrate particular relationships. For example, at 1 GPa the projection from Di–Hd illustrates the initiation of melting at the six-phase [Ol + Opx + Cpx + Sp(Cr–Al) + Plag + Liq] cotectic. The composition of plagioclase at the solidus (which is determined by bulk composition and *P, T*) will control the solidus *T* and melt composition [9, 10]. With plagioclase eliminated, increasing melt fraction moves smoothly from [Ol + Opx + Cpx + Sp(Cr < Al)] saturation to [Ol + Opx + Sp (Cr > Al)] saturation. With further melting, orthopyroxene is eliminated and melts lie on olivine control lines passing through the bulk composition, i.e. HPY or MPY in Fig. 1. However, in the projection from Ol (Fig. 1b), the different trends of six-phase, five-phase (Plag absent), four-phase (Plag + Cpx absent) and three-phase cotectics (Plag + Cpx + Opx absent) are clearly separated. In many models of mantle upwelling, approaching adiabatic decompression, melt is envisaged as percolating by porous flow from within a melting volume until aggregation of these melt increments into dunite channels or dykes (magma segregation). As long as melts are in porous flow through lherzolite, the projections illustrate the roles of pressure, bulk composition and melt fraction in re-equilibrating melt composition. Alternatively, melts may be trapped within an upwelling ‘plume’ or ‘diapir’ which has a significant temperature gradient from diapir core to ambient enclosing mantle. The diapir is ‘sealed’ by the solidus temperature until the melt escapes through dykes or dunite channels, i.e. approaching batch melting. As noted previously, in addition to the residual phase assemblage control, the partitioning of compatible elements represented in solid solutions must also match between melts and residual minerals, for example Mg–Fe in olivine and pyroxenes; Ca–Na in plagioclase and clinopyroxene; and Cr–Al in spinel and pyroxenes.

In Fig. 1 illustrating the experimentally determined melt compositions for two model mantle compositions, the HPY composition is an ‘enriched’ mantle composition (a ‘pyrolite’ model mantle calculated from Hawaiian olivine tholeiite) and MPY is a ‘fertile’ or ‘asthenospheric’ mantle composition (a ‘pyrolite’ model mantle calculated from a mid-ocean ridge tholeiite composition). Of the two lherzolite compositions, HPY has higher normative Di–Hd component (higher Ca/Al) and higher incompatible elements, particularly K, Ti, P, C and H. The effects of C and H on melting are particularly important and differ with oxidation state, i.e. whether carbon is present as CO<sub>2</sub> or carbonates, dissolved in melts as (CO<sub>3</sub>)<sup>2–</sup>, as graphite or diamond or as CH<sub>4</sub> in reduced fluid phase. The Fe<sup>3+</sup> content of Cr–Al spinel acts as a sensor for *f*O<sub>2</sub> and indicates that Hawaiian ‘hot-spot’ and other IB have higher *f*O<sub>2</sub>

than MORB [11, 12]. In both cases, carbon is soluble in silicate melts as carbonate and thus the solution of both water and carbonate have the effect of lowering solidus temperatures, changing melt compositions at the solidus and lowering liquidus temperature of a given melt composition.

## 2.2 A simple system analogue for peridotite + C, H, O

It is helpful to illustrate the importance of dissolved (CO<sub>3</sub>)<sup>2–</sup> and (OH)<sup>–</sup> and of *f*O<sub>2</sub> on lherzolite melting by considering the simple system forsterite (Mg<sub>2</sub>SiO<sub>4</sub>) + nepheline (NaAlSi<sub>3</sub>O<sub>8</sub>) + quartz (SiO<sub>2</sub>). This simple system [13–15] is part of the basal plane of the basalt tetrahedron. The system contains liquidus fields for olivine and orthopyroxene, the major phases of the upper mantle. At low pressure, the beginning of melting of a simple albite-bearing harzburgite occurs at the [albite (Ab) + forsterite (Fo) + enstatite (Ens) + melt] invariant point. For peridotitic compositions, increase in temperature produces liquids lying on the Fo + Ens cotectic until Ens is eliminated, and higher-temperature liquids then lie on an olivine control line to the bulk composition. At high pressure, albite is replaced by the clinopyroxene, jadeite, and the positions of the invariant point (solidus: Jd + Fo + Ens + Melt) and the (Fo + Ens + Melt) cotectic are shown at 2.8 GPa (Fig. 2). Melt at the invariant point is strongly Ne normative, melting is incongruent, and the melting reaction is Fo + Jd → Ens + (Ne)<sub>melt</sub>. Higher-temperature melts on the (Fo + Ens + Melt) cotectic remain Ne normative up to very Fo-rich

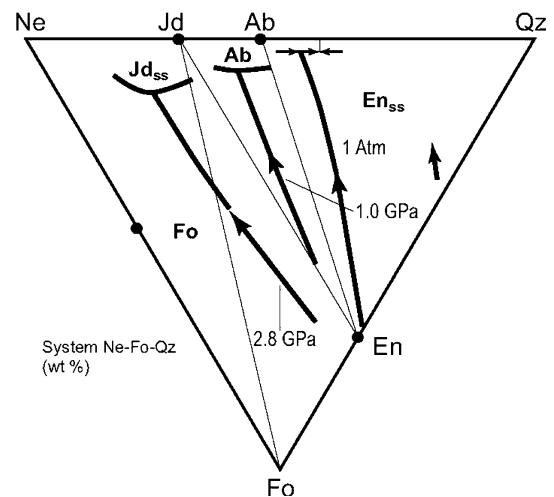


**Fig. 2** Phase diagram for the system nepheline–forsterite–quartz (wt%). Liquidus fields, cotectics and four-phase peritectic points (‘harzburgite’ solidi) at 1 bar, 1 and 2.8 GPa. At 1 bar (Ol + Ens + Liq 1 → Ens + Ab + Liq 2), at 1 GPa (Ol + Ens + Liq 3 → Ol + Ab + Liq 4) and at 2.8 GPa (Ol + Ens + Liq 5 → Ol + Jd + Liq 6) (reproduced from [13, 73])

compositions. Referring to Fig. 3, the intersection of the (Fo + Ens + Melt) cotectic with a compositional join, such as (Ab—Fo<sub>45</sub>Ne<sub>55</sub>), is an indicator of the degree of silica undersaturation of the melt ('basalt') in equilibrium with harzburgite residue. Compositions along the join (Ab—Fo<sub>45</sub>Ne<sub>55</sub>) were studied with C, O, H fluids under controlled  $fO_2$  conditions and the melt and vapour compositions determined by electron microprobe and gas chromatography/mass spectrometry (GCMS). At 2.8 GPa, melting of jadeite-bearing harzburgite begins at 1,365 °C in the absence of water or carbon. With increasing temperature, liquids lie on the Fo + Ens + melt peritectic and this crosses the (Ab—Fo<sub>45</sub>Ne<sub>55</sub>) join at 1,490 °C [13]. The melt composition is strongly nepheline normative, i.e. it lies in the Ne + Jd + Fo field. If excess water is added, the field of olivine expands at the expense of enstatite and melting begins at much lower temperature. Melts along the Fo + Ens + Melt + H<sub>2</sub>O cotectic cross the (Ab—Fo<sub>45</sub>Ne<sub>55</sub>) join at 1,120 °C, and this melt is more silica rich and less nepheline normative than that under dry melting conditions. In the presence of CO<sub>2</sub>, i.e. with C present and at high  $fO_2$  and dry conditions, the Fo + Ens + Melt + CO<sub>2</sub> peritectic is displaced towards the Fo + Ne join and crosses the (Ab—Fo<sub>45</sub>Ne<sub>55</sub>) join at 1,410 °C. The melt composition is extremely nepheline and olivine rich, approaching 'olivine nephelinite'. These experiments illustrate the opposing effects of H<sub>2</sub>O and CO<sub>2</sub>—although both lower the melting temperatures under oxidising conditions, H<sub>2</sub>O moves melts towards more silica-saturated

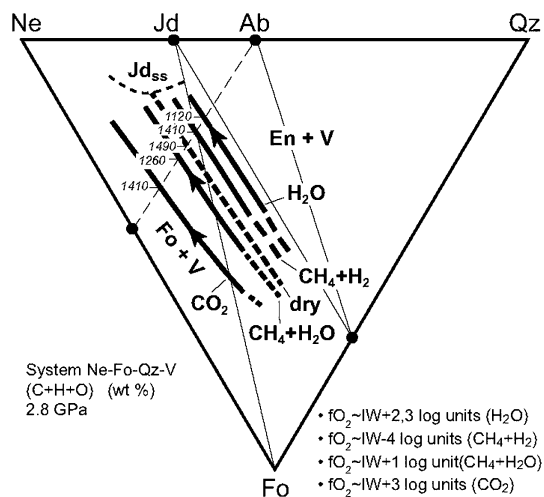


**Fig. 3** System nepheline–forsterite–quartz at 2.8 GPa with C, H, O vapour at different oxygen fugacities. The boundary (cotectic) between enstatite and forsterite as liquidus phases was located by experiments on compositions lying on the join (albite to Ne55–Fo45). The positions of the cotectic with (C, H, O) vapour components at different  $fO_2$  buffers are shown relative to the C, H-absent cotectic (Fig. 2) with temperatures of the intersections indicated (reproduced from [14, 15, 73])

compositions, whereas CO<sub>2</sub> drives melts to more olivine- and nepheline-normative compositions.

As carbon can be present as carbonate, CO<sub>2</sub>, graphite or diamond, or as CH<sub>4</sub>, it is necessary to consider the role of oxygen fugacity ( $fO_2$ ). In the absence of variable valence in Fe, Ti or Cr in the simple system, the effects of external buffering at different  $fO_2$  are expressed in different C, H, O behaviour. At extremely reducing conditions using aluminium carbide + aluminium hydroxide to generate CH<sub>4</sub>-rich fluid (estimated  $fO_2 \sim IW-3$ , 4 log units [14]), the Fo + Ens + melt peritectic boundary crosses the (Ab—Fo<sub>45</sub>Ne<sub>55</sub>) join at  $\sim 1,410$  °C at a composition between the dry and water-saturated boundaries and a temperature 80 °C lower than the C, H-free system. FTIR spectroscopy demonstrated small dissolved (OH)<sup>−</sup> and carbon contents [14, 15] (even at these extremely reducing conditions). Later experiments in the Ne + Fo + Qz system used graphite capsules and tungsten carbide/tungsten oxide (WCWO) external buffer to generate carbon-saturated CH<sub>4</sub> + H<sub>2</sub>O fluid at  $fO_2 \sim IW + 1$  log unit [16]. For these conditions at 2.8 GPa, the Fo + Ens + melt peritectic boundary intersects the (Ab—Fo<sub>45</sub>Ne<sub>55</sub>) join at 1,260 °C. The intersection is very close in normative composition to the dry intersection at 1,490 °C. FTIR spectroscopy shows (OH)<sup>−</sup> and (CO<sub>3</sub>)<sup>2−</sup> absorption bands and analysis of the fluid (capsule piercing and GCMS analysis) obtained approximately 1:4 molar ratio of methane to water in the vapour phase [16]. The melt contains  $\sim 6$  wt% H<sub>2</sub>O and 0.6 wt% dissolved CO<sub>2</sub>. This study shows that in the peridotite analogue, albite-bearing harzburgite, a methane + water fluid in equilibrium with graphite at 2.8 GPa and  $fO_2 \sim IW + 1$  log unit caused depression of the liquidus of a melt coexisting with olivine and orthopyroxene by 230 °C by dissolved (OH)<sup>−</sup> and (CO<sub>3</sub>)<sup>2−</sup> and with little change in melt composition (calculated water and CO<sub>2</sub> free).

### 2.3 Peridotite + C, H, O

The same effect was demonstrated by Odling et al. [17] for the HPY composition and reduced (C, O, H, S) fluid. The experiments were fluid saturated [(H<sub>2</sub>O + CH<sub>4</sub>) fluid] and buffered by graphite and the tungsten carbide/tungsten oxide buffer which at these conditions is at  $fO_2 \sim IW + 1$  log unit. At 2 GPa, 1,175 °C HPY composition is above the solidus and the melt dissolved approximately 7 % H<sub>2</sub>O and 1.3 % CO<sub>2</sub>. It is picritic in composition with  $\sim 16$  % MgO and is hypersthene normative. The melt comprises  $\sim 20$ –25 modal% of the HPY composition and leaves residual olivine (44 modal%), orthopyroxene (27 %), clinopyroxene (7 %) and sulphide (1 %). The melt and residue compositions are closely similar to the melt and residue compositions found in anhydrous melting of the

HPY composition at 2 GPa, 1,450–1,500 °C (14 %–16 % MgO, 25 %–30 % melt [18]). At  $fO_2 \sim IW + 1$  log unit and in equilibrium with graphite, melting is fluxed by carbon and hydrogen, lowering equivalent degrees of melting by  $\sim 250$  °C with little change in melt composition [17]. At these low  $fO_2$  conditions (which are appropriate to MORB and OIB sources), dissolved carbon, as carbonate, and dissolved water have opposite, but roughly balancing effects on melt composition. In both the simple system analogue and the enriched lherzolite composition (HPY), dissolved carbonate (equivalent to only 1 %–2 %  $CO_2$ ) shifts the Ol + Opx cotectic to more olivine-rich and more silica-undersaturated compositions, but this shift in the position of the Ol + Opx cotectic is reversed by solution of  $(OH)^-$  (equivalent to  $\sim 7$  %  $H_2O$ ). Carbon-free, water-saturated melting of the HPY composition at 2 GPa, 1,100 °C [17, 19] yielded a similar melt fraction (27 %), but the melt has 12.6 % MgO and has much lower normative olivine (see Fig. 4) and higher water content ( $\sim 15$  wt%–20 wt%).

Melting studies of simple system analogues, and of lherzolite model mantle, show that solution of both water and  $CO_2$  strongly modify melt compositions in equilibrium with olivine and enstatite at pressures above 1 GPa. The effects are opposite, solution of  $CO_2$  driving melts to lower silica contents, and higher olivine and normative nepheline

contents. Solution of water drives melts towards higher silica contents. The role of  $fO_2$  is extremely important in stabilising graphite or carbonate at higher  $fO_2$  and in controlling the fluid composition ( $CH_4 + H_2O > H_2$ ) at lower  $fO_2$  in the presence of graphite or diamond. Most importantly, at mantle  $fO_2 \sim IW + 1$  log unit at 2.5–3.5 GPa [15–17] carbonate is not stable and, assuming carbon and/or water exceed the storage capacity of crystalline phases, then fluid in equilibrium with graphite is dominantly  $(CH_4 + H_2O)$ . This fluid causes depression of the lherzolite solidus by  $\sim 250$  °C, and near-solidus melts contain dissolved  $(OH)^-$  and  $(CO_3)^{2-}$ . The simple system Ne + Fo + Qz is a useful analogue for demonstrating the fluxing effects of both water and carbonate in depressing the solidus at pressures greater than the carbonation reactions of  $CO_2$  with olivine  $\pm$  clinopyroxene.

In both the analogue system and the HPY composition, carbon and hydrogen have significant solubility in melts at  $fO_2 \sim IW + 1$  log unit, and flux melting when the sub-solidus fluid is approaching pure water or water + methane, in equilibrium with graphite or diamond. Melts produced at these  $fO_2$  conditions at 2–3 GPa have essentially all iron as FeO, but carbon dissolved as  $(CO_3)^{2-}$ . Also melt compositions (calculated  $H_2O$ - and  $CO_2$ -free) are very similar to anhydrous and carbonate-free melts at a given melt fraction but are at  $\sim 250$  °C lower temperature.

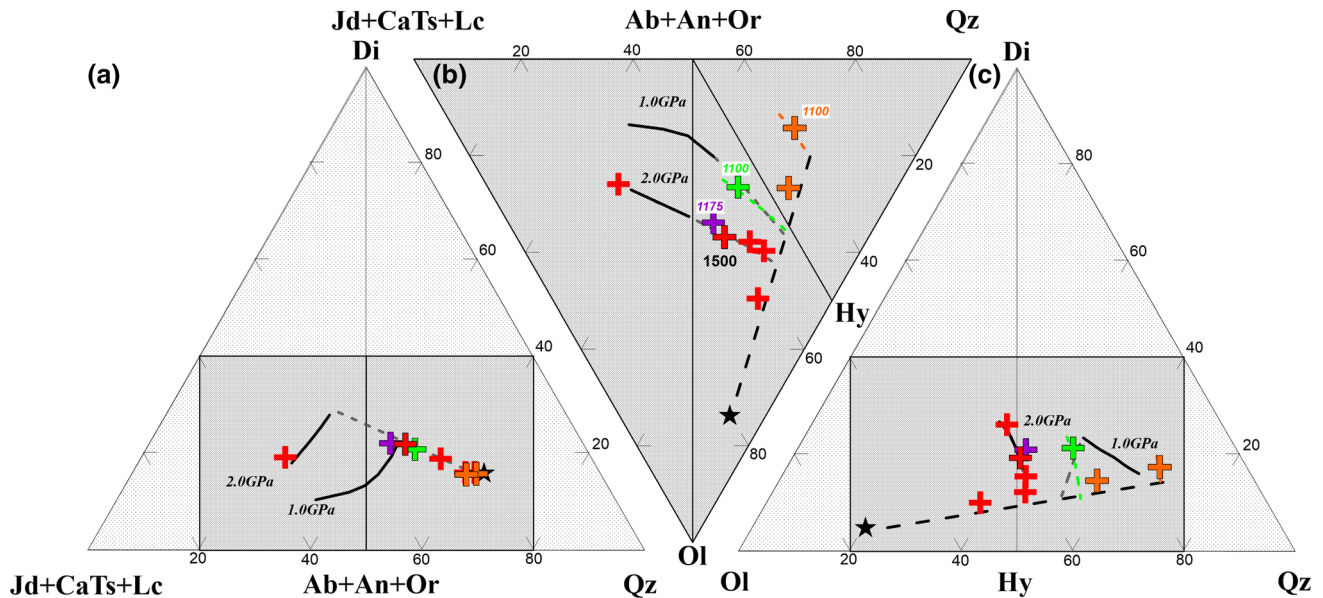


**Fig. 4** (Color online) The ‘basalt tetrahedron’ projections of Fig. 1 are used to illustrate the melt compositions in HPY lherzolite under dry and carbon-free conditions (red crosses and black lines) at 2 GPa and 1,500 °C,  $\sim 25$  %–30 % melting leaving clinopyroxene-bearing harzburgite residue [18]. In comparison, the water-saturated, carbon-free, melt at 2 GPa and 1,100 °C (green cross) is much lower in normative olivine (b, c) [19]. Most importantly, the composition of a similar melt fraction (purple cross) with dissolved  $(OH)^-$  and  $(CO_3)^{2-}$  at low  $fO_2$  ( $\sim IW + 1$  log unit) at 2 GPa 1,175 °C [17] is overlapping with the C, H-absent melt at 1,500 °C. The figure illustrates effects similar to those in the simple system (Figs. 2, 3), i.e. at low  $fO_2$  ( $\sim IW + 1$  log unit) solubility of  $(OH)^-$  and  $(CO_3)^{2-}$  in basaltic melts lowers liquidus temperatures by  $\sim 300$  °C, but the melt composition, calculated volatile-free, is close to that under dry and carbon-free conditions. Also the harzburgite cotectic under C, H-absent conditions and at 1 GPa (black line) is compared with C-absent, water-saturated melts at 1 GPa (orange crosses [19])

### 3 Primary magmas inferred from mid-ocean ridge glass compositions

There is now a large database of MORB glass compositions (petdb.ldeo.columbia.edu), and from this database, 190 glasses with  $>9.5$  wt% MgO are plotted in Fig. 5 [20]. In Fig. 5a, the projection from olivine, most glasses lie on the 1.5–1.8 GPa lherzolite residue trend or on the 1–2 GPa harzburgite residue trend, and it is important that they do not lie on or close to the plagioclase lherzolite residue trend. A few glasses plot below the 1 GPa lherzolite trend, and equally a few glasses plot in the 2–2.5 GPa lherzolite field. This projection gives no indication of differences in normative olivine content, but very few glasses lie in the silica-undersaturated field. Figure 5b shows differences in olivine content of the glasses which are tightly clustered and trend towards the quartz apex. Relative to the lherzolite partial melting trends, many indicate pressures of 1 GPa or less. Olivine is the low-pressure liquidus phase for all compositions, and addition of olivine, particularly to the more siliceous glasses, is required to reconcile the pressure estimations from the two projections. Also, the Mg# of the glasses is too low for equilibrium with residual mantle

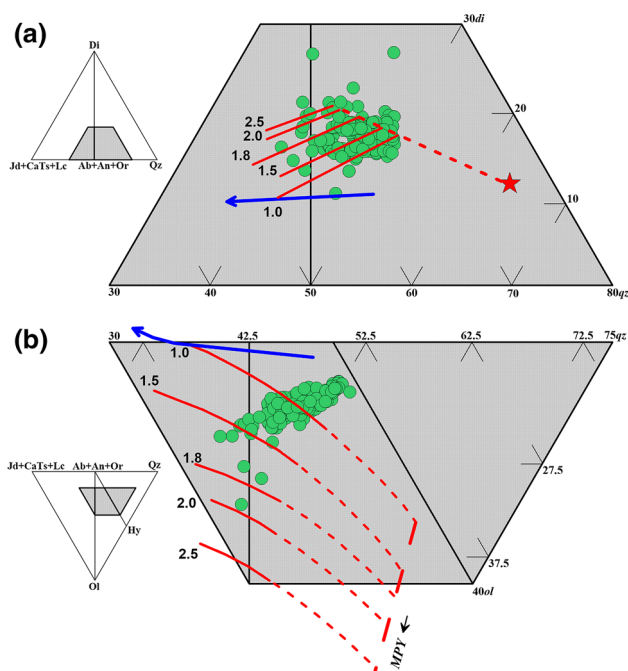


**Fig. 5** (Color online) Compositions of  $\sim 190$  MgO-rich glasses from the 'Petrological Data Base of the Sea Floor' (petdb.ldeo.columbia.edu) projected into the 'basalt tetrahedron' as an overlay to the partial melting trends for MPY at pressures from 1 to 2.5 GPa [20]. Glasses have  $>9.5$  wt% MgO. The thick arrow intersecting the low-temperature end of the 1 GPa lherzolite residue trend marks the appearance of plagioclase and the locus of melt in six-phase equilibria (Ol + Opx + Cpx + Plag + Cr–Al spinel + melt) in which plagioclase is  $\sim \text{An}_{80}$  at the hypersthene-normative end and  $\sim \text{An}_{40}$  at the arrowhead in nepheline-normative field [9, 10]

olivine of  $\text{Fo}_{90-91}$ , and addition of olivine would produce compositions consistent with both multiple phase saturation (Ol + Opx  $\pm$  Cpx  $\pm$  Sp) and Mg/Fe partition constraints for a lherzolitic mantle source.

Independent evidence for low-pressure olivine crystallisation and separation is provided by the presence of olivine phenocrysts and microphenocrysts of higher Mg# than the liquidus olivine for the analysed glass, commonly with rare Al–Cr spinel. Unfortunately, few studies which report glass compositions provide analyses of microphenocrysts. Green et al. [21] identified eight glasses with microphenocrysts up to  $\text{Fo}_{91.5-92.1}$  in glasses for which liquidus olivine was  $\text{Fo}_{86.9-89.9}$ . They calculated parental or primary magmas by incrementally adding liquidus olivine to each glass until the calculated liquidus olivine matched the observed microphenocrysts (using PETROLOG [22]). The calculated parent magmas were picritic with 13.0 %–15.6 % MgO.

One of the high-MgO glasses from the Mid-Atlantic Ridge (DSDP 3-18-7 [23]) with 10.1 % MgO was studied experimentally (Fig. 6) [24]. Olivine is the liquidus phase to 1.2 GPa where it is joined and then replaced at higher

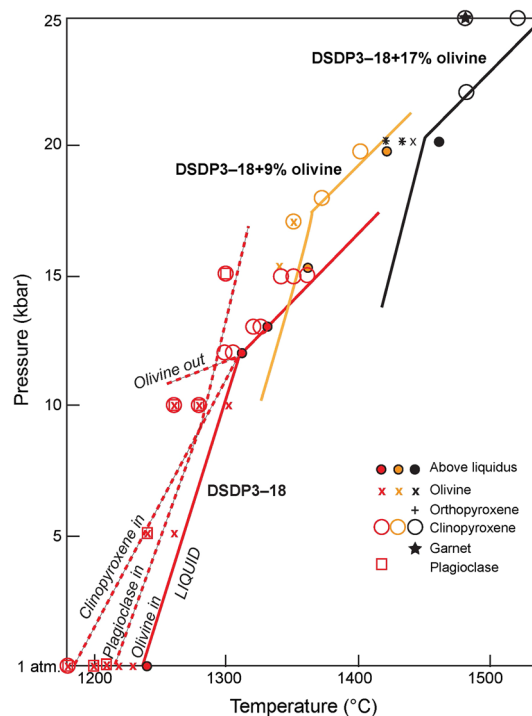


**Fig. 6** (Color online) Experimental determination of liquidus and near-liquidus phases for olivine tholeiite glass DSDP3-18-7-1 and two olivine-enriched compositions with 9 % and 18 % added olivine. Plagioclase at low pressure and clinopyroxene at  $>1$  GPa follow olivine below the liquidus, and clinopyroxene replaces olivine as liquidus phase with increasing pressure except at 2 GPa in the most olivine-rich composition. In this composition, olivine and orthopyroxene are liquidus and near-liquidus phases at 2 GPa, 1,420–1,440  $^{\circ}\text{C}$  [24]

pressure by calcic clinopyroxene. Experiments with added orthopyroxene showed that the composition was removed from orthopyroxene saturation at or above 1.2 GPa. Addition of ~15 % olivine yielded a tholeiitic picrite (~16 % MgO) which was saturated with olivine (Fo<sub>91.5</sub>) and orthopyroxene at 2 GPa, 1,420–1,430 °C.

In a later study, Green and Falloon [20] used glasses with >9.5 wt% MgO [190 examples from the database (Petrological Database of the Sea Floor: petdb.ldeo.columbia.edu)]. These were projected into the basalt tetrahedron and compared with the partial melting trends for MPY. The compositions are strongly grouped around the 1–2 GPa lherzolite to harzburgite residue in the projection from olivine. In detail, different ridge localities plot at slightly different positions in the projections, but in all cases, addition of olivine to the observed glass was required to reconcile the pressures of (Ol + Opx) saturation inferred from the two projections. Glasses from the

Galapagos Ridge and calculated parent magmas are plotted in Fig. 7 (Fig. 10 in [20]) and lie on the 1.5 GPa melting trends with lherzolite–harzburgite residues. Figure 7 shows three groups of glass compositions and primary magmas segregating at 1.5 GPa from (Ol + Opx + Cpx ± Sp) residue (Groups A and B) and (Ol + Opx ± Sp) residue (Group C). The residues would have olivine of Fo<sub>89</sub>, Fo<sub>89.5</sub> and Fo<sub>90.5</sub>, respectively, consistent with different degrees of melting at 1.5 GPa.

Falloon et al. [25] examined in detail three representative magmatic suites from mid-ocean ridge settings (Cocos-Nazca, East Pacific Rise and Mid-Atlantic Ridge). They used both glass and olivine phenocryst compositions and included volatile (H<sub>2</sub>O) contents to constrain the most Mg-rich melt. Olivine was incrementally added to the glass compositions to obtain a liquid in equilibrium with the most magnesian olivine phenocryst. Liquidus temperatures were calculated as 1,243–1,351 °C at 0.2 GPa (Table 1) including the effect of very small dissolved volatiles (H<sub>2</sub>O, CO<sub>2</sub>). In addition, experimental peridotite reaction experiments at 1.8 and 2.0 GPa, using the most magnesian of the calculated parental MORB liquids (Cocos-Nazca) confirmed (Ol + Opx + Cpx) saturation at this pressure. The depths of multiple saturation of other MORB parental liquids were estimated as 1–2 GPa from the MPY melting trends in the basalt tetrahedron.

Using the 0.2 GPa liquidus temperatures of the parental MOR picrites, we can estimate the *P*, *T* for magma segregation at multiple saturation with olivine + orthopyroxene (+clinopyroxene) from the liquid adiabat and the melt fraction (required to estimate latent heat of melting [6]). The inferred melt fraction derives from mass balance of assumed source, and residue and parental magma compositions. For fertile lherzolite source such as MPY or HZ, the melt fraction for the parental picrites is ~15 %–25 % melt. From these steps, the mantle potential temperature (*T*<sub>p</sub>) beneath mid-ocean ridges ranges from 1,320 to 1,490 °C [25] (*T*<sub>p</sub> is the temperature at 1 bar from an olivine adiabat drawn from the intersection of the adiabatically upwelling mantle *P*, *T* path with the anhydrous solidus for dry lherzolite, or the intersection with ~1 % melt contour for MPY with trace water). In a later section, we estimate that *T*<sub>p</sub> for ‘hot-spot’ tholeiite sources (Hawaii, Iceland and Réunion) ranges from 1,502 °C (Réunion) to 1,565 °C (Hawaii) [25]. The differences in *T*<sub>p</sub> values between the hottest MORB and ocean island tholeiite sources are ~75 °C, significantly less than predicted by the thermally driven mantle plume hypothesis. The higher *T*<sub>p</sub> for the ‘hot-spot’ sources is estimated because the model source HPY requires ~30 %–35 % melting to yield the parental picrites and harzburgite residues. This model based on HPY composition thus requires a larger latent heat of melting than the MOR picrites from MPY, leaving clinopyroxene-bearing harzburgite residue. The

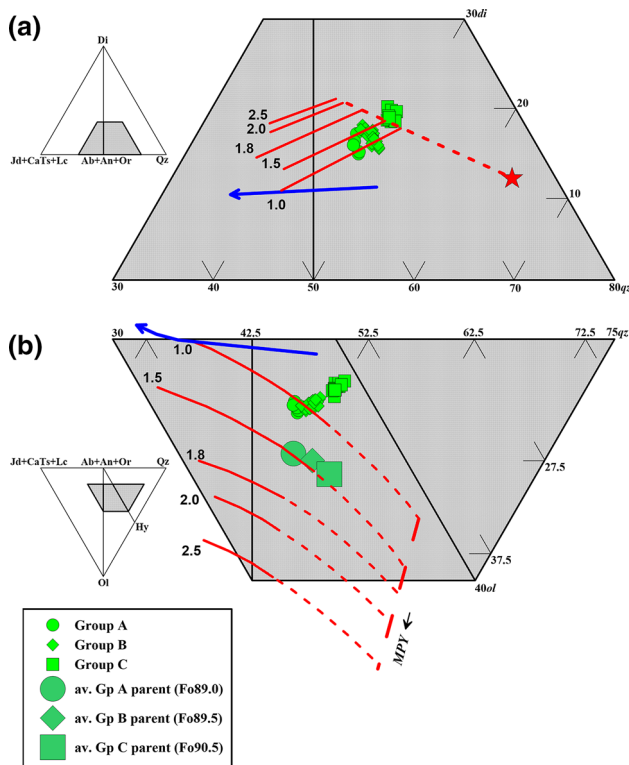


**Fig. 7** (Color online) Compositions of MgO-rich glasses from the Galapagos Ridge from the ‘Petrological Data Base of the Sea Floor’ (petdb.ldeo.columbia.edu) selected from Fig. 5 and projected into the ‘basalt tetrahedron’. The glasses can be grouped—Groups A and B are in the lherzolite residue field at 1.3–1.5 GPa (a) with Group B indicating a higher melt fraction from MPY source relative to Group A. Group C is the most SiO<sub>2</sub> rich and plots at the clinopyroxene-out cusp (a) at 1.5 GPa. Olivine addition calculations suggest parental magmas plotting on the 1.5 GPa cotectic with clinopyroxene-bearing residue for parental magmas A and B, and harzburgite residue for parent C. Residual (liquidus) olivines for the parental magmas were calculated at Mg# of 89, 89.5 and 90.5 for a–c, respectively [20]

**Table 1** Calculated model parental liquids at 0.2 GPa

| No.<br>Sample name             | Kilauea    |             |              |             |            | Mauna Loa<br>6<br>182-7 | Reunion<br>7<br>REg | MORB      |            |            | Iceland<br>11<br>NO42 |
|--------------------------------|------------|-------------|--------------|-------------|------------|-------------------------|---------------------|-----------|------------|------------|-----------------------|
|                                | 1<br>S-5 g | 2<br>57-11c | 3<br>57-13 g | 4<br>57-15D | 5<br>57-9F |                         |                     | 8<br>896A | 9<br>D20-3 | 10<br>Vema |                       |
| SiO <sub>2</sub>               | 47.24      | 47.53       | 48.01        | 48.48       | 50.44      | 48.74                   | 46.23               | 47.70     | 48.29      | 49.36      | 47.00                 |
| TiO <sub>2</sub>               | 2.03       | 1.62        | 1.73         | 1.83        | 2.02       | 1.67                    | 2.31                | 0.54      | 0.86       | 0.83       | 0.64                  |
| Al <sub>2</sub> O <sub>3</sub> | 10.21      | 9.59        | 10.04        | 10.54       | 11.95      | 10.30                   | 10.98               | 13.46     | 15.25      | 17.17      | 13.03                 |
| Fe <sub>2</sub> O <sub>3</sub> | 1.58       | 1.80        | 1.64         | 1.51        | 1.12       | 1.54                    | 1.51                | 0.85      | 0.69       | 0.51       | 1.40                  |
| FeO                            | 9.96       | 10.77       | 10.26        | 9.78        | 8.05       | 9.38                    | 9.91                | 8.56      | 7.69       | 6.68       | 8.15                  |
| MnO                            | 0.15       | –           | –            | –           | –          | 0.12                    | 0.15                | 0.10      | 0.12       | 0.12       | 0.15                  |
| MgO                            | 16.79      | 18.80       | 17.86        | 17.00       | 14.00      | 17.53                   | 16.17               | 15.86     | 13.93      | 10.86      | 16.75                 |
| CaO                            | 9.03       | 7.59        | 7.92         | 8.28        | 9.46       | 8.22                    | 8.73                | 11.44     | 10.88      | 12.03      | 11.37                 |
| Na <sub>2</sub> O              | 1.67       | 1.39        | 1.49         | 1.55        | 1.81       | 1.66                    | 2.02                | 1.36      | 2.16       | 2.24       | 1.34                  |
| K <sub>2</sub> O               | 0.39       | 0.25        | 0.29         | 0.29        | 0.32       | 0.24                    | 0.59                | 0.02      | 0.02       | 0.06       | 0.03                  |
| P <sub>2</sub> O <sub>5</sub>  | 0.20       | 0.17        | 0.18         | 0.18        | 0.20       | 0.15                    | 0.22                | 0.03      | 0.04       | 0.05       | 0.07                  |
| Cr <sub>2</sub> O <sub>3</sub> | –          | –           | –            | –           | –          | –                       | –                   | 0.06      | –          | –          | –                     |
| H <sub>2</sub> O               | 0.76       | 0.49        | 0.57         | 0.56        | 0.62       | 0.46                    | 1.18                | 0.04      | 0.06       | 0.10       | 0.08                  |
| Mg#                            | 75.0       | 75.7        | 75.6         | 75.6        | 75.6       | 76.9                    | 74.4                | 76.8      | 76.3       | 74.3       | 78.6                  |
| Temp. <sup>a</sup>             | 1,335      | 1,372       | 1,355        | 1,341       | 1,286      | 1,354                   | 1,323               | 1,351     | 1,320      | 1,243      | 1,361                 |
| Oliv. eq. <sup>b</sup>         | 90.70      | 90.70       | 90.70        | 90.70       | 90.70      | 91.30                   | 90.65               | 91.60     | 91.50      | 90.50      | 92.40                 |
| % Oliv. <sup>c</sup>           | 17.6       | 15.7        | 8.6          | 12.4        | 11.0       | 23.1                    | 22.7                | 16.3      | 10.3       | 3.4        | 17.5                  |

Based on most MgO-rich glasses and olivine phenocryst cores [25]

Table 2 in [25] Parental magmas calculated from MgO-rich glasses by olivine addition calculations performed with software PETROLOG [22]

<sup>a</sup> Calculated olivine liquidus temperature (°C) at 0.2 GPa using the models of Ford et al. [28] and Falloon et al. [25]

<sup>b</sup> Calculated equilibrium olivine composition at the 0.2 GPa liquidus temperature

<sup>c</sup> Wt% olivine added incrementally to glasses to estimate parental magma with liquidus olivine matched to most MgO-rich phenocryst cores

difference disappears if the hot-spot magmas are derived by smaller degrees of partial melting of a refertilised refractory source.

To summarise current investigations of melt compositions from mid-ocean ridges, glasses with >9.5 % MgO have olivine and Al–Cr spinel as liquidus phases, but the Mg# of liquidus olivines is lower than in model mantle compositions. Phase relationships at high pressure, partition relationships of compatible elements (Fe, Mg, Ni) and evidence from some examples with olivine phenocrysts of Mg# >89, argue for primary tholeiitic picrite magmas with 13 %–16 % MgO, liquidus olivine to Fo<sub>91.5</sub> and liquidus spinel of Cr# = 20–50. Liquidus temperatures are reduced by 20–30 °C at depth due to dissolved (H<sub>2</sub>O, CO<sub>2</sub>), and eruption temperatures of primary MOR magmas are 1,240–1,350 °C. Melting and melt extraction from residual mantle is in the spinel lherzolite stability field, leaving clinopyroxene-bearing harzburgite at pressures most commonly between 1.5 and 2 GPa. For a fertile source such as MPY or HZ [26], the degree of melting to yield residual clinopyroxene-bearing harzburgite to clinopyroxene-free harzburgite at ~1,430 °C, 1.5–2 GPa is 15 wt%–25 wt%. The high degree of melting and nature of residual phases (olivine, aluminous orthopyroxene, aluminous, subcalcic and Na-

poor clinopyroxene, and Al–Cr spinel) means that the melting process significantly alters compatible trace element abundances and ratios but effectively partitions all incompatible elements into the melt phase, with little or no change in incompatible element ratios. The corollary of this is that the differences in incompatible element ratios which are observed among MORB are properties of the source and not of the actual melting and melt extraction processes assigned to mantle upwelling and melt extraction beneath mid-ocean ridges. Thus, the distinctions based on incompatible trace element ratios which characterise D-MORB (depleted), N-MORB ('normal') and E-MORB (enriched) are attributed to processes within the asthenosphere, prior to upwelling, or for E-MORB possibly also by a 'wall-rock reaction' metasomatism during diapiric upwelling or in dunite-channel transport after melt segregation.

#### 4 Primary magmas inferred from Hawaiian tholeiitic glass compositions

The Hawaiian volcanic chain is the most studied example of a 'hot-spot' magma province, and characteristically each volcanic centre has a major cone-building phase in which

the magmas are olivine tholeiites, followed by transition to alkali olivine basalts and derivative, fractionated hawaiites and mugearites. On the older, western islands, small and younger volcanic centres are silica-undersaturated olivine basanite, olivine nephelinite and olivine melilitite, including some with mantle-derived xenolith suites. An important paper by Norman and Garcia [27] examined picritic magmas from the main cone-building phase of six volcanoes and demonstrated that the calcium content of olivine (at a common Mg#) correlated with the magma composition, varying from Loihi with high-Ca and Koolau at the low-Ca end. In addition, the most magnesian olivines were  $\geq \text{Fo}_{88}$  in all cases and up to  $\text{Fo}_{91.5}$  for Mauna Loa. These relationships between olivine and magma established that the olivines were phenocrysts and not xenocrysts from disrupted mantle and that parental magmas were picritic with 15 %–16 % MgO. Also a picrite was dredged offshore from Kilauea with glass containing 14.7 % MgO and olivine phenocrysts to  $\text{Fo}_{90.7}$  [27]. These data enable calculation of parental magmas matched to the most magnesian olivine observed [20, 21, 25, 27]. The experimentally derived ‘olivine thermometer’ [28] is then used to estimate anhydrous liquidus temperatures for parental picrites of each volcanic centre. When plotted in the basalt tetrahedron, these picrites lie closer than the MOR picrites to the Ol–Qz side of the projection from Di and are thus in the harzburgite residue rather than lherzolite residue field in terms of phase equilibria constraints on mantle-derived melts (Fig. 8). In the projection from olivine, they define harzburgite residue trends but individually pointing back to different source ‘pyrolite’ compositions, i.e. Loihi lies on the harzburgite trend for the HPY composition, Kilauea, Mauna Loa, Hualalai and Kohala lie on a trend with lower Di (Ca/Al) and Koolau is distinctively lower again. These compositional characteristics are reinforced if glass compositions from melt inclusions trapped in olivine phenocrysts are included [20, 25, 29]. Falloon et al. [25] estimate the parent magma for Kilauea (Puna rift submarine eruption) as having 17 wt%–18 wt% MgO and eruption temperature of 1,340–1,355 °C, which includes liquidus depression by 0.5 wt%–0.6 wt% H<sub>2</sub>O. Finally, the Hawaiian Scientific Drilling Project sampled ~3 km of fresh tholeiitic lavas from Mauna Kea cone-building stage and provided an extensive database of glass compositions. Selecting compositions with olivine and Cr–Al spinel as phenocrysts, the large majority of glasses with >7 % MgO fall into two compositional groups—a low SiO<sub>2</sub> (48.5 %–49 %) group and a high SiO<sub>2</sub> (51 %–52 %) group [30]. The two groups of glasses are tightly clustered, each with a harzburgite residue trend in the projection from Ol in the basalt tetrahedron, and spread along Ol-control lines in the projection from Di (Fig. 9). Stolper et al. [30] recognised the evolved nature of the glasses and calculated parental

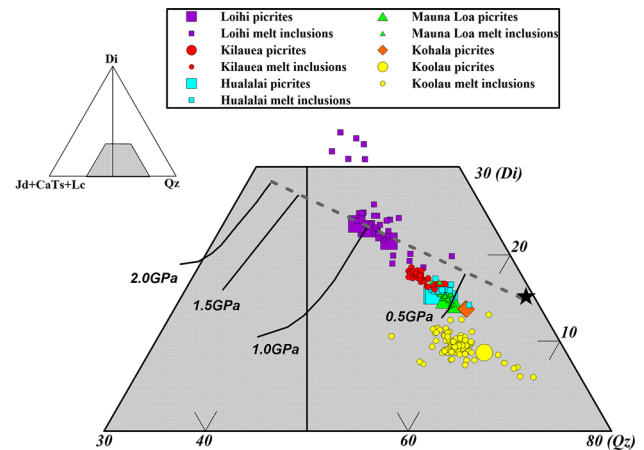


**Fig. 8** (Color online) Compositions of inferred parental magmas from different Hawaiian volcanoes projected from Ol on to the Di + (Jd + CaTs + Lc) + Qz face of the ‘basalt tetrahedron’. Parental picrites [27] are shown by large symbols, and melt inclusions with >8 % MgO, in olivine, are shown by small symbols [29]. The melt inclusions overlap the picrite compositions for each volcano and illustrate trends parallel to the ‘harzburgite residue’ trend of melts at high melt fraction in HPY. As has been demonstrated experimentally for the Kilauean picrite [31–34], it is inferred that the parental picrites for each volcano left residual harzburgite (Ol + Opx + Cr–Al spinel), but sources/residues differed slightly from higher Ca/Al for Loihi to lower Ca/Al for Koolau [20]

picrite compositions to be in equilibrium with  $\text{Fo}_{90.5}$  olivine. Also differences in composition imply a slightly higher Ca/Al in the source for the high SiO<sub>2</sub> group and incompatible element, and isotopic differences also emphasise source differences for the two groups [30]. Plotting the glass compositions within the basalt tetrahedron suggests slightly lower degree of melting for the low SiO<sub>2</sub> group parent. Using the melting constraints for HPY composition, a preferred model suggests that the parent magma for the low SiO<sub>2</sub> group was picrite (15.6 % MgO) which separated from residual harzburgite with  $\text{Fo}_{90}$  at 2 GPa. Similarly, the parental picrite (15.7 % MgO) for the high SiO<sub>2</sub> parent magma separated from harzburgite with  $\text{Fo}_{90.5}$  at 1.5 GPa [20]. Stolper et al. [30] recognised additional glass populations in the Mauna Kea lavas, distinguished by both major and minor element compositions (at ~1,800 m; at ~2,235 m; and alkali olivine basalts as the uppermost lavas). The use of the basalt tetrahedron projections [20] suggests a higher Ca/Al source and lower melt fraction, but also with harzburgite residue, for the parental lavas at ~1,800 m depth. The parental magmas for the lavas at ~2,235 m indicate a similar source to the major low SiO<sub>2</sub> group, harzburgite residue but lower melt fraction [20, 30]. If the mantle source has 3 %–4 % CaO and Al<sub>2</sub>O<sub>3</sub> and Mg# ~90 (i.e. similar to HPY), then consistency with harzburgite residue would require the low SiO<sub>2</sub> parent to represent ~20 % melting, the high SiO<sub>2</sub> parent to represent ~25 % melting and the unit at 2,235 m

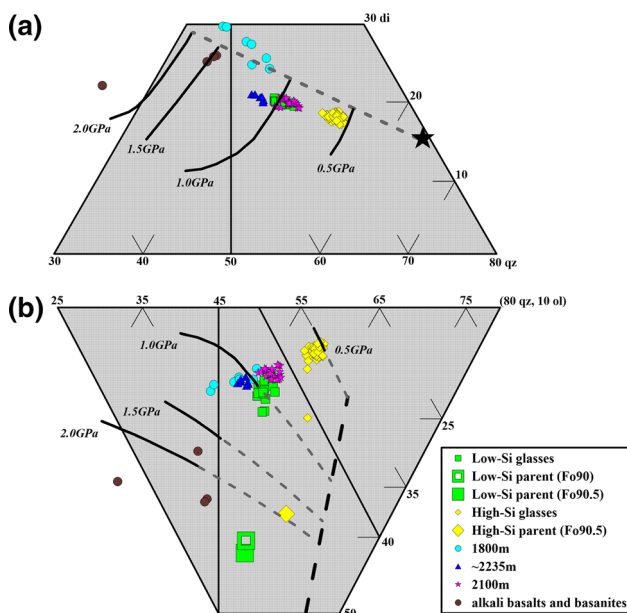


**Fig. 9** (Color online) Glass compositions from Mauna Kea cone-building lavas, sampled by the Hawaiian Scientific Drilling Project [30] projected onto faces of the ‘basalt tetrahedron from olivine (a) and diopside (b), respectively. The ‘high-SiO<sub>2</sub>’ [30] glasses selected have >7.25 % MgO, and those from the ‘low-SiO<sub>2</sub>’ glasses have >8 % MgO. Other glasses recognised as of distinctive compositions at depths of 1,800 and 2,235 m depth also plot in coherent groups. Three alkali basalts and a basanite plot appropriately in the nepheline-normative field. **b** Estimated parental magmas calculated by Stolper et al. [30] for the ‘low-SiO<sub>2</sub>’ and ‘high-SiO<sub>2</sub>’ groups, assuming residual olivine with Mg# = 90.5 (green square and yellow diamond), together with an alternative parental magma for the ‘low-SiO<sub>2</sub>’ calculated assuming residual olivine of Mg# = 90 (open square) [20]

to represent 14 % melting. The uppermost lavas encountered in the drilling project include three alkali olivine basalts (units 45, 47) and an olivine basanite (unit 58). If K<sub>2</sub>O and P<sub>2</sub>O<sub>5</sub> are perfectly incompatible and the source is very similar to that for the low SiO<sub>2</sub> group, then the parental olivine basanite is a product of 6 %–7 % melting and the alkali olivine basalts are produced by ~10 % melting. The lower melt fractions also require higher pressure and lherzolite rather than harzburgite residues [20]. If, rather than a source lherzolite with 3 %–4 % CaO and Al<sub>2</sub>O<sub>3</sub>, a depleted source with ~1.5 %–2 % CaO and Al<sub>2</sub>O<sub>3</sub> is chosen, then the same sequence of melt compositions will form as functions of melt fraction and pressure, but the range of melt percentage will be from 3 % to 12.5 % rather than 6 %–25 %, and the change of Mg# in the residue as a consequence of melt extraction will be much less—illustrating the interplay of the phase equilibria (eutectic style melting) and element partitioning (solid solution, compatible elements) and also implying the source effect on estimation of latent heat of melting.

A consistent picture for Hawaiian parental magmas emerges from examination of picrites (olivine and glass

compositions) for different volcanoes; of melt inclusions in olivine phenocrysts; and from glasses from ~3-km section through Mauna Kea lavas. During the main cone-building phase of each volcano, high degrees of melting (12 %–25 %, assuming a lherzolite-to-harzburgite source composition which is more refractory than HPY or HZ) and depths of magma segregation at 1.5–2 GPa leave clinopyroxene-free harzburgite residues. However, source compositions are not constant but vary in major and minor element composition, including variable Ca/Al, and are depleted, i.e. approaching harzburgite, rather than lherzolitic in major element composition. This would be consistent with liquidus spinel with Cr# ~60 in Hawaiian picrites [27] compared with 20–50 for MORB. The requirement for source heterogeneity is reinforced by incompatible element abundances, by fractionation among incompatible elements and by variation in isotopic ratios. In Hawaiian tholeiites, the characteristic enrichment in LREE and LILE and depletion in HREE, relative to MORB or to chondritic abundances, have commonly been attributed to element fractionation during partial melting, implying low degrees of melting and residual garnet, i.e. high pressures and <5 % melting leaving garnet lherzolite residue. This is clearly inconsistent with the experimental studies of Hawaiian picrites and the previous discussion emphasising harzburgite residues and large melt fractions. Experimental high-pressure studies of Hawaiian olivine tholeiite, olivine basalt, picrite and alkali olivine basalt [31–34] demonstrate the absence of garnet as a liquidus phase below 3.5 GPa and that the olivine tholeiite to tholeiitic picrite magmas with 13 %–17 % MgO have only olivine, orthopyroxene and Cr–Al spinel as liquidus phases to 3–3.5 GPa. Enrichment and fractionation among incompatible elements is attributed to prior events and processes affecting the source (Fig. 8) or to wall-rock reaction processes which extract near-solidus melts (incipient melts) from larger volumes of cooler or deeper mantle (Fig. 10) [25, 34, 35]. The compatible element characteristics, particularly increase in Cr/Al, Mg/Fe, Ca/Al, and depletion in HREE, are also suggestive of earlier melt extraction followed by refertilisation event(s) in the ‘hot-spot’ sources.

To summarise current investigations of melt compositions from Hawaiian ‘hot-spot’ magmas, glasses with >7 %–8 % MgO have olivine and Al–Cr spinel as liquidus phases. However, olivine phenocryst compositions extend to Fo<sub>89</sub> or Fo<sub>91.3</sub> in particular volcanic centres, and addition of olivine leads to parental tholeiitic picrite magmas with 14 %–17 % MgO, liquidus olivine to Fo<sub>91.3</sub> and liquidus spinel of Cr# = 60–75. Anhydrous liquidus temperatures of primary Hawaiian magmas are 1,356–1,442 °C but are reduced by 60–80 °C at depth due to dissolved (H<sub>2</sub>O, CO<sub>2</sub>). Melting and melt extraction from residual mantle is in the spinel

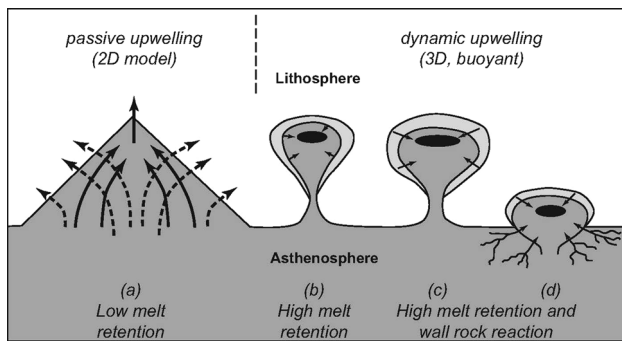


**Fig. 10** Diagram illustrating several processes which may be significant in mantle upwelling, decompression melting and magma segregation in MOR and intraplate settings [35, 73]. **a** Melt and residue paths in passive upwelling of asthenospheric lherzolite beneath the mid-ocean ridge to form new lithosphere. Melt compositions are in local equilibrium with residual lherzolite–harzburgite and thus vary throughout the melting volume. Melt flow is focussed and melt fraction increases until separation from residues and transition from porous flow to flow through dunite channels or basaltic dykes. **b–d** Dynamic upwelling of ‘diapirs’, ‘thermals’ or ‘plumes’ in response to super-adiabatic temperature gradient in the uppermost mantle and rheological and density variation through the lithosphere and asthenosphere. The asthenosphere contains incipient carbonate-bearing hydrous silicate melt with low permeability at <1 %–2 % melt fraction. As diapirs rise through the lithosphere the melt fraction will increase if temperatures within the diapir approach adiabatic cooling. However, increasing temperature contrast between diapir and the geothermal gradient in the lithosphere may cause marginal crystallisation with inward migration of near-solidus melt (**b**). In **c**, the lithospheric wall-rock may be heated above its solidus (particularly if it contains pargasite, phlogopite and/or carbonate) and incipient melt move into the diapir (wall-rock reaction). Marginal entrainment of wall-rock may also occur in the dynamo-thermal aureole of the diapir. In **c**, incipient melt within the asthenosphere may access a diapir sourced from underlying mantle

lherzolite stability field, leaving clinopyroxene-free harzburgite at pressures most commonly between 1.5 and 2 GPa. For an enriched or fertile source such as HPY or MPY, the degree of melting to yield residual clinopyroxene-free harzburgite at  $\sim 1,400$  °C, 1.5–2 GPa is 15 wt%–25 wt%, or a lower melt fraction if depleted lherzolite to harzburgite is the source composition. The high degree of melting and nature of residual phases (olivine, aluminous orthopyroxene and Al–Cr spinel) means that the melting process significantly alters compatible trace element abundances and ratios but effectively partitions all incompatible elements into the melt phase, with little or no change in incompatible element ratios. The corollary of this is that the heterogeneity in incompatible element ratios observed in tholeiitic Hawaiian parental magmas is a property of the source and not of the actual melting and melt extraction processes during mantle upwelling and melt extraction. Thus, the variations in incompatible trace element ratios and isotopes which characterise Hawaiian volcanic centres are attributed to processes within or beneath the asthenosphere, prior to upwelling and melt segregation, together with

enrichment from possible wall-rock reaction in magma channels (Fig. 10).

## 5 Primary intraplate magmas (non-‘hot-spot’)

### 5.1 Basaltic and nephelinitic magmas

Intraplate basaltic volcanism also occurs within continental rifts, areas of crustal thinning and lithospheric stretching, and as seamounts, including recently identified areas of young, small eruptions on old oceanic crust adjacent to ocean trenches [4]. Silicate magmas are diverse from quartz tholeiites to olivine nephelinites, lamproites and olivine melilitites and also as evolved (low Mg#) hawaiites, mugearites, trachytes and phonolites. The selection of ‘primary’ magma compositions for experimental testing is based firstly on magmas which contain xenoliths of mantle origin (density >3.3 g/cc). Such magmas have clearly acquired their compositions by upper mantle processes but include melts which are not primary in the sense of liquids derived by partial melting of mantle peridotite, but are fractionated melts following high-pressure crystallisation (commonly evidenced by megacrysts including aluminous pyroxenes, olivine, kaersutitic and pargasitic hornblende, garnet and more rarely apatite, anorthoclase, andesine, phlogopite). Experimental studies of such fractionated melts demonstrated the important role for pargasitic to kaersutitic amphibole in controlling crystal fractionation in the upper mantle producing evolved magmas including nepheline mugearites to phonolites [36–39].

‘Primary’ magmas are selected from among the xenolith-bearing magmas by restriction to magmas with  $Mg\# = 70–75$ , i.e. having liquidus olivine with  $Mg\# = 89–93$ . The liquidus phases of high-Mg# xenolith-bearing magmas have been explored at high pressure and temperature, seeking conditions of multiple saturation by  $Ol + Opx \pm Cpx \pm Ga$  or  $Sp$ . Alkali olivine basalt to picrite (normative  $Ol + Plag$  with minor  $Ne$ ) may be derived by low degrees of melting with spinel lherzolite residue at 1–2 GPa [31]. A particular example from Auckland ID, NZ, contained megacrysts of olivine ( $Fo_{87}$ ), aluminous enstatite and aluminous clinopyroxene. Experimental study [40] demonstrated that all three phases occurred on or very close to the liquidus at 1.1–1.2 GPa,  $\sim 1,310$  °C, but the extent of mutual solid solution between the pyroxenes in the anhydrous experiments was much greater than that shown by the megacryst pairs. Addition of  $\sim 2$  wt%  $H_2O$  depressed the liquidus temperature by  $\sim 120$  °C and yielded liquidus pyroxenes matching the natural megacryst compositions at 1.4–1.5 GPa,  $\sim 1,180$  °C. Further evidence for the role of water in lowering liquidus temperatures, expanding the compositional gap between

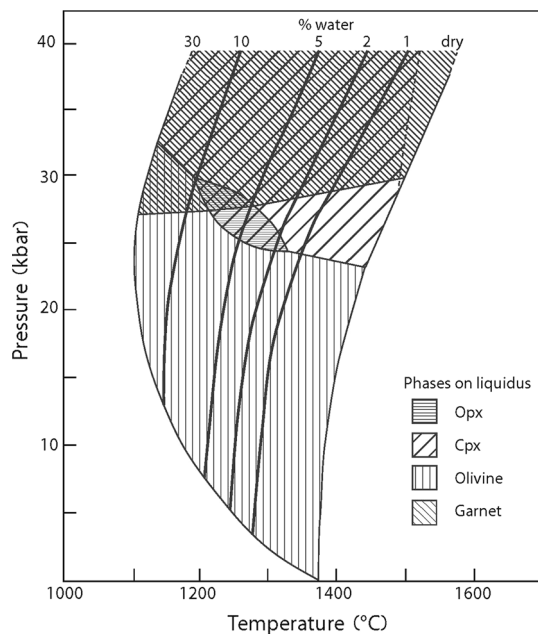


**Fig. 11** Diagram illustrating the effect of pressure to increase water solubility and liquidus depression in an olivine-rich basanite (xenolith-bearing, mantle-derived magma). Liquidus for the indicated water contents were interpolated from bracketing the liquidus for a range of water contents from 0.5 wt% to 25 wt% H<sub>2</sub>O [39, 41]. The *P*, *T* fields over which olivine (low pressure), clinopyroxene, garnet and orthopyroxene appeared on the liquidus are shown. The olivine-rich basanite has orthopyroxene on or near the liquidus over limited *P*, *T* and water content and is a partial melt leaving residual garnet lherzolite at 2.5–3 GPa, 1,150–1,250 °C [39, 41]

ortho- and clino-pyroxenes and extending the liquidus field for Ol + Opx into more silica-undersaturated olivine-rich basanites, was found in the study of olivine-rich basanite from south-western Victoria, Australia [41]. Under dry conditions, olivine, followed by clinopyroxene, was the liquidus phases with increasing pressure and orthopyroxene did not appear near the liquidus. The liquidus phase fields were explored, varying pressure, temperature and water contents (Fig. 11). The maximum solubility of water (to ~30 wt%) and the consequent depression of liquidus temperature (~350 °C) increased with pressure up to ~3 GPa. The *P*, *T* field for olivine as the liquidus phase expands to higher pressure with increasing water content and olivine is followed by clinopyroxene, or garnet at low temperature and water contents >10 wt% approx (Fig. 11). A field for orthopyroxene as a liquidus phase was found between ~2 wt% H<sub>2</sub>O and 10 wt% H<sub>2</sub>O, pressures of 2.5–3 GPa and temperatures of 1,300–1,200 °C. These experiments did not contain added carbon (carbonate), but additional experiments were conducted in graphite capsules with excess fluid and products included Ol + Opx + glass (Fig. 2 of [41]), with the glass estimated to contain >5 wt% H<sub>2</sub>O and significant dissolved (CO<sub>3</sub>)<sup>2-</sup> [42]. The experimental study suggested that at pressures of 2.5–3 GPa,

melting of garnet lherzolite could be fluxed by water so that at temperatures of ~1,250 °C, the melt composition at 6 %–8 % melting was olivine-rich basanite leaving garnet lherzolite residue [41, Table 5].

The search for conditions for Ol + Opx ± Cpx ± Ga saturation at high pressure was continued with studies on olivine nephelinite [43], olivine melilitite [42, 44, 45] and a K-rich lamprophyre [46]. These studies showed that although pressure increased the solubility of water, expanded the liquidus field of olivine and depressed the liquidus temperatures, Ca-rich clinopyroxene remained the second phase to crystallise at lower pressure and replaced olivine as liquidus phase at higher pressure. For these strongly silica-undersaturated magmas, orthopyroxene was not a liquidus or near-liquidus phase under dry conditions or with added water. The olivine melilitite composition (a xenolith-bearing intraplate volcanic plug from Tasmania, emplaced during rifting and early separation of Antarctic and Australian plates) was systematically explored at pressures to 4 GPa, varying both H<sub>2</sub>O and CO<sub>2</sub> contents [42, 44, 45]. It was shown that olivine, orthopyroxene, clinopyroxene and garnet were liquidus phases at pressures of 2.5–3 GPa, 1,100–1,200 °C, provided both H<sub>2</sub>O and CO<sub>2</sub> were present. For the specific magma studied, the four-phase saturation is around 2.7 GPa, 1,170 °C with ~6 %–7 % CO<sub>2</sub> and 7 %–8 % H<sub>2</sub>O in solution [45]. Adam [47] explored the liquidus phases of alkali-rich olivine basanite and olivine nephelinite with H<sub>2</sub>O and CO<sub>2</sub> and inferred four-phase saturation at 2.6–3.5 GPa, 1,150–1,200 °C with approx 6 wt% dissolved volatiles. Similarly, for the K-rich lamprophyre composition, multiple saturation with Ol + Opx + Cpx + Phlog occurs at ~1,250 °C, 3 GPa, provided both H<sub>2</sub>O and CO<sub>2</sub> are present [48].

By combining the experimental study of the liquidus phases of intraplate mantle-derived magmas (the inverse approach) with phase stabilities during melting of fertile or enriched lherzolite (MPY, HZ or HPY) at high pressure (the forward approach), the problem of quench modification of melts and difficulty of determining melt composition at small melt fraction was addressed. A petrogenetic grid (Fig. 12b) expresses *P*, *T*, H<sub>2</sub>O and CO<sub>2</sub> contents for genesis of primary intraplate magmas from olivine melilitite to olivine tholeiite—this petrogenetic grid uses major and minor element contents and the control of magma compositions by equilibrium phase relations (Figs. 1–3 of [49]; [50, 51]). The model was applied to the Tertiary–Recent volcanic province of SW Victoria and tested by use of trace element abundances with emphasis on rare earth elements (REE) because of the range of incompatibility shown from LREE to HREE [52]. It was demonstrated that the range of primary magmas from olivine melilitite to olivine tholeiite could be produced by 4 % to ~25 % melting of lherzolite HPY, with the more undersaturated magmas segregating from garnet lherzolite residues at pressure of ~2.5–3 GPa.

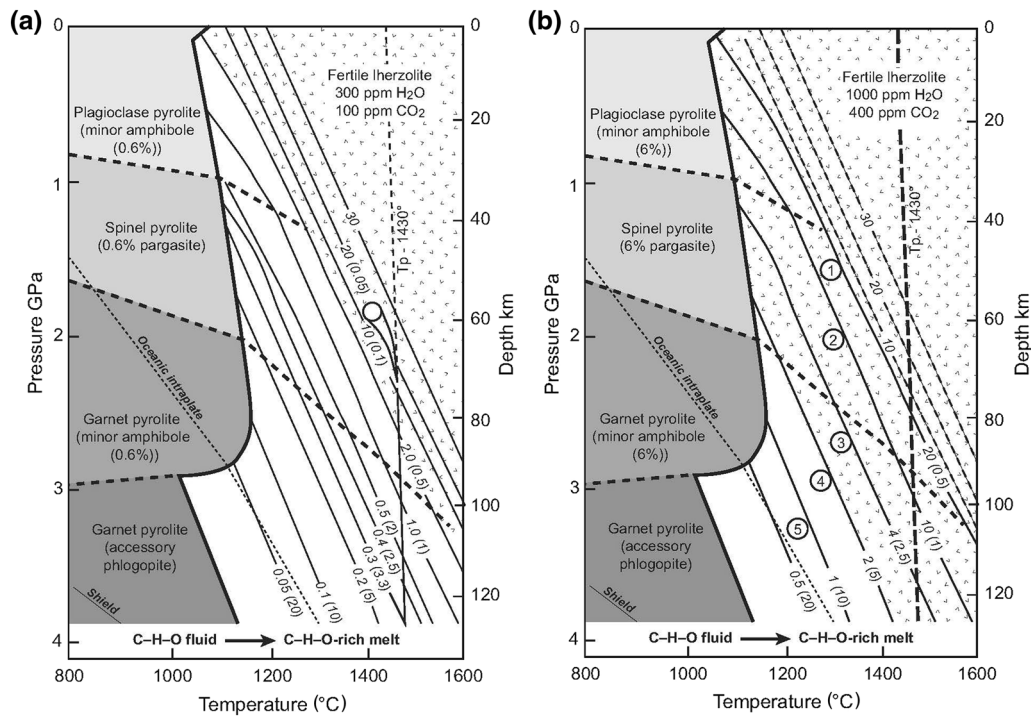


**Fig. 12** Major melting and incipient melting regimes for fertile (MPY) and enriched (HPY) lherzolites with assumed water and CO<sub>2</sub> contents [20, 73]. **a** Solidus and melting parameterisation for model MORB source mantle with 300 ppm H<sub>2</sub>O and 100 ppm CO<sub>2</sub>, mantle potential temperature ( $T_p$ ) of ~1,430 °C. Contours show % melt and approximate dissolved water content of melt (in brackets). A permeability threshold (sharp increase) at ~2 % melting contour is marked by shading. Parental MOR picrite from ~15 % to 20 % melt at ~2 GPa, 1,420 °C. **b** Solidus and melting parameterisation for model intraplate (enriched-HPY) mantle with 1,000 ppm H<sub>2</sub>O and 400 ppm CO<sub>2</sub>, mantle potential temperature ( $T_p$ ) of ~1,430 °C. Solid line contours show % melt from 0.5 % to 20 % and approximate dissolved water content of melt (in brackets). Shaded area denotes >2 % melt. Dashed line contours refer to MORB source mantle, i.e. a comparison with the HPY source. Primitive and mantle xenolith-bearing basalts from SE Australia are plotted at inferred depths of melt segregation: 1 olivine tholeiite, 2 alkali Ol. basalt, 3 Ol-rich basanite, 4 Ol-nephelinite, 5 Ol-melilitite-nephelinite [47, 52]

Garnet disappears as a residual phase with increasing melt fraction and decreasing pressure of magma segregation. Melt compositions change smoothly through olivine basanite, alkali olivine basalt to olivine tholeiite. A major conclusion from the attempt to reconcile major element compositions and phase relationships with trace element abundances was that for this magmatic province, a common source composition must be an ‘enriched’ lherzolite (such as HPY). The ‘enriched’ character of the intraplate magma source included higher H<sub>2</sub>O, CO<sub>2</sub>, P<sub>2</sub>O<sub>5</sub> and K<sub>2</sub>O contents and higher  $fO_2$  than the MORB source. The spectrum of primary mantle-derived basaltic magmas from olivine melilitite to olivine tholeiite could not be derived from a source which had chondritic or N-MORB relative abundances of incompatible elements, particularly REE. The study re-enforced the conclusion from the studies of Hawaiian olivine tholeiites and MORB that differences in relative abundances among incompatible elements could not be explained by differences in melting conditions of a common upper mantle source but required a separate process, commonly a precursor process, of enrichment or depletion in incompatible elements. The nature of the

enrichment/depletion process suggested addition or loss of an incipient, near-solidus melt such as carbonatite or carbonate-bearing hydrous silicate melt.

A major feature of melting in the upper mantle which evolved from the ‘forward’ and ‘inverse’ experimental studies of basalt and mantle melting was the distinctive solidus (in  $P, T$  space) and the key roles for (C, H, O). It was assumed that the water contents of olivine, pyroxenes and garnet (NAMs) were negligible and that water contents as low as ~100 ppm would stabilise pargasite to the solidus up to 3 GPa and would initiate melting at the water-saturated solidus at higher pressures. New experimental studies of simple systems, and of natural minerals, argued for relatively large water contents in NAMs of source lherzolite. A number of workers inferred that the water contents observed in both MORB and ‘hot-spot’ basalts could be stored in NAMs, negating the importance of pargasite at the solidus and using inferred  $c_{residue}/c_{melt}$  to predict the mantle solidus for various water contents [53, 54].

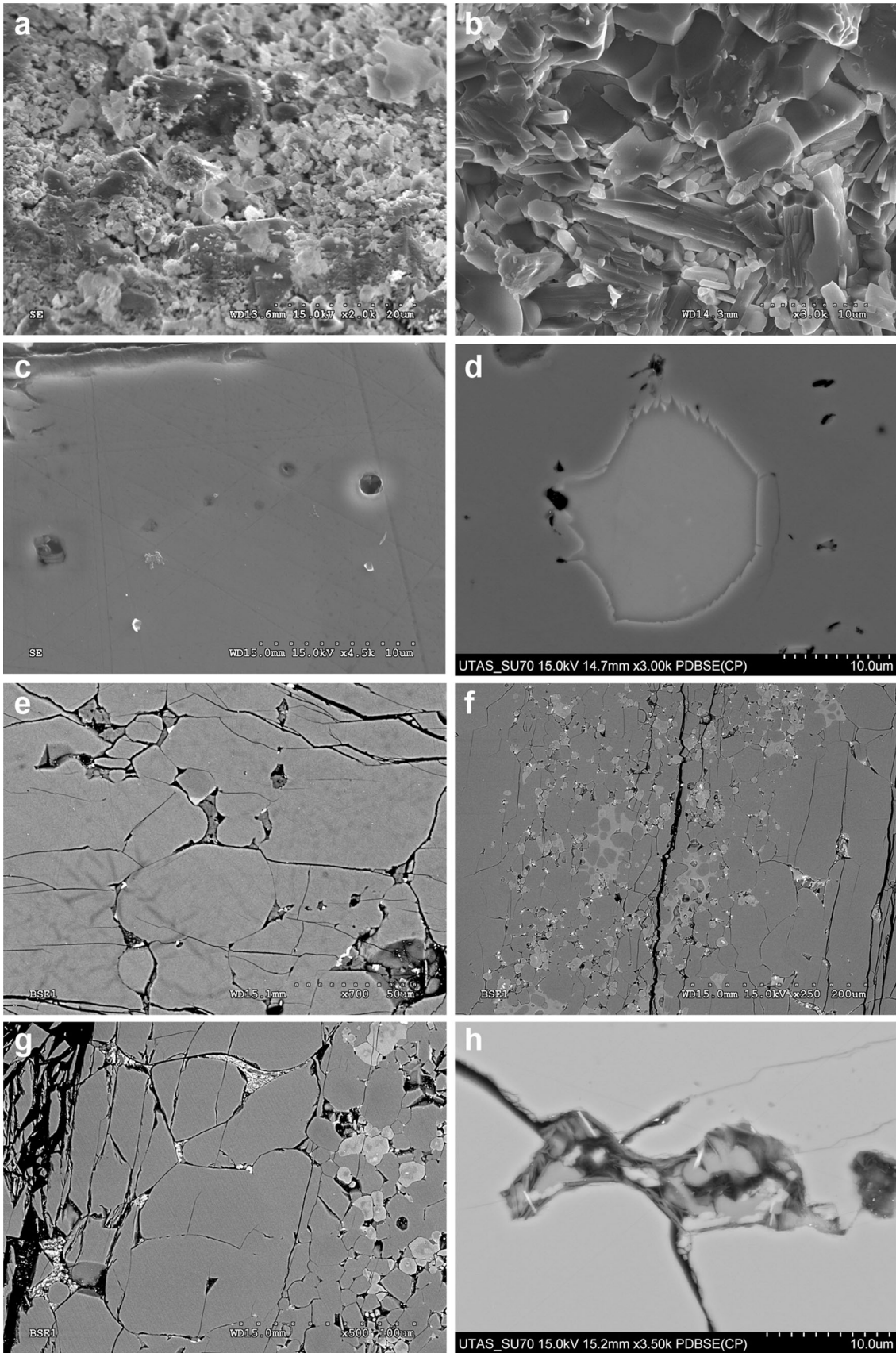
In addition to the debate on water in NAMs, a recent study [55, 56] redetermined the solidus for Lherzolite + H<sub>2</sub>O

(+CO<sub>2</sub>) at fluid-saturated conditions to 6 GPa, using the model mantle composition HZ [26] which is very close to MPY. This experimental study used very high water contents (14.5 wt%) and inferred a very low solidus temperature ( $\sim 810$  °C from 3 to 6 GPa), restriction of pargasite stability to  $<2$  GPa and appearance of chlorite at the solidus. The authors regarded earlier work as incorrect and applied their results to interpret melting regimes and to model melting in fluid-rich environments at convergent margins.

Arising from these two debates (i.e. the role of water partitioning in NAMs and the  $P$ ,  $T$ , dependence of the water-saturated solidus), a new experimental study was designed with polycrystalline olivine layers as a melt trap for very small melt fractions [51, 58, 59]. The layers of olivine (or orthopyroxene or clinopyroxene) were analysed by Fourier transform infrared spectroscopy (FTIR) to determine water contents and partitioning of water between melt, fluid or hydrous mineral (pargasite, phlogopite) and nominally anhydrous minerals (NAMs—i.e. olivine, orthopyroxene, clinopyroxene). By analysing quenched melt interlocks (Fig. 13d–h), the compositions of very small melt fractions close to the solidus were shown to be transitional between olivine melilitite and sodic, dolomitic carbonatite (1.5 %–2 % melt) and alkali-rich olivine nephelinite to olivine basanite (2 %–4 % melt). Melt compositions at 2.5 GPa had higher Na/Ca than at 4 GPa reflecting increase in  $(\text{Na}/\text{Ca})_{\text{Cpx}}/(\text{Na}/\text{Ca})_{\text{Melt}}$  with increasing pressure. The stability of pargasite (Na, K and Ti-bearing amphibole) at the water-saturated solidus to pressure of 3 GPa was confirmed, as was the distinctive shape of the dehydration solidus for small water contents (up to 3,000–4,000 ppm H<sub>2</sub>O). The temperature of the vapour-saturated solidus decreases with increasing pressure to 970 °C at 1.5 GPa, but then increases through 1,025 °C at 2.5 GPa, 1,225 °C at 4 GPa and 1,375 °C at 6 GPa (Fig. 14) [57]. The experimental study demonstrated the limited solubility of water in olivine and pyroxenes (NAMs) under upper mantle conditions and the dominant role for pargasite in the water storage capacity of lherzolite in the lithosphere (Fig. 14) [51]. Arrows in Fig. 14 indicate pressures at which the vapour-saturated solidus (hydrous silicate melt) was determined. Panel at right plots the water storage capacity of fertile, MORB source mantle (i.e. MPY or HZ Lherzolite) as a function of depth, along the vapour-saturated solidus. At  $<100$  km approx., pargasite is stable to the solidus, but the modal abundance of pargasite reaches a maximum at 1–1.5 GPa and decreases towards higher pressure [60]—hence the water storage capacity decreases with modal pargasite. Pargasite becomes unstable at  $>3$  GPa, and water storage capacity drops to that ( $\sim 200$  ppm) which can be retained in NAMs in fertile lherzolite.

**Fig. 13** Scanning electron microscope images of high-pressure, high-temperature experiments illustrating techniques used to establish the lherzolite solidus in the presence of known water contents and very small carbonate and to obtain mineral and melt compositions. **a** Lherzolite HZ at 2.4 GPa, 960 °C with 14.5 wt% water. Euhedral olivine with disaggregated, thin films of glass quenched from vapour/fluid phase. Subsolidus with  $\sim 30$  vol% water-rich vapour, pargasite absent due to vapour-phase leaching, particularly of K, Na, Si. **b** Lherzolite HZ at 2.4 GPa, 960 °C with 1.45 wt% water. Euhedral olivine, orthopyroxene, clinopyroxene, garnet and pargasite with porous texture and uncommon flakes of quenched glass films (vapour-phase quench). Subsolidus with  $\sim 3$  vol% water-rich vapour, pargasite stable. **c** Lherzolite HZ at 2.5 GPa, 1,000 °C with 7.25 wt% water. Linear array of vapour-phase bubbles in healed fracture in olivine disc placed within lherzolite HZ. Vapour-phase bubbles contain fragments of vapour-phase quench. Subsolidus with  $\sim 15$  vol% water-rich vapour; pargasite absent due to vapour-phase leaching. **d** Lherzolite HZ at 2.5 GPa, 1,450 °C under ‘dry’ conditions. Quenched melt (glass) is within an olivine ‘melt-trap layer and in intersertal texture with glass enclosed by multiple olivine faces, i.e. not at ‘triple-points’. Olivines show quench outgrowths (Fe rich), and glass is chemically zoned. The melt composition is extracted from multiple area scans including glass, quenched olivine outgrowths and melt-trap olivine (known composition), treated as olivine + melt mixtures. **e** Lherzolite HZ at 6 GPa, 1,300 °C with 1.45 wt% water and very small carbonate content. Quenched carbonatite melt (Fe-rich dolomite + Fe oxide) in intersertal texture in olivine melt-trap layer. Below-solidus for hydrous silicate melt, above solidus for carbonatite. **f** Lherzolite HZ at 6 GPa, 1,400 °C with 1.45 wt% water and very small carbonate content. The image shows the HZ garnet lherzolite layer between melt-trap olivine to left and right. The upper olivine layer (to the right) shows large interlocks of quenched carbonate-bearing hydrous silicate melt of olivine melilitite composition (36 % SiO<sub>2</sub>, 18 % CaO). Above solidus for Lherzolite HZ, hydrous silicate melt with significant dissolved carbonate at  $f_{\text{O}_2} \sim \text{IW} + 1-2$  log units. **g** Lherzolite HZ at 6 GPa, 1,400 °C with 1.45 wt% water and very small carbonate content. Quench texture of silicate, carbonate and oxide from carbonated hydrous silicate melt trapped in olivine layer. Lherzolite layer to right of image. **h** Lherzolite HZ at 2.5 GPa, 1,025 °C with 1.45 wt% water and very small carbonate content. Quench phases (silicates, oxides and carbonate) in melt intersert in olivine layer. Images **f–h** are all above the solidus for mantle lherzolite +(C–H–O) [51, 58, 59]. **i** Layered experiment to test whether a proposed primary melt (usually a composition obtained from a forward experiment in which a lherzolite has been run at the same  $P$ ,  $T$ , and the residual minerals analysed and melt composition calculated) is correct. The picritic layer (22 wt% of the charge) is equilibrated with the lherzolite, and consistency of the residual phases with those of the forward experiment is confirmed. The large area of quenched glass is not modified by the quench outgrowths on primary phases. Exp. 4,280; basaltic glass + MM3 lherzolite at 1 GPa, 1,325 °C. Residual phases are Ol + Opx + Cpx + spinel [81]. **j** As in (i) except experiment T-2086 is at higher  $P$  (2.5 GPa) and  $T$  (1,550 °C), so that quench outgrowths are large and only a small fraction of the original melt layer is preserved. Upper layer was tholeiitic picrite (DSDP3-18) (21 wt% of charge), and lower layer was MPY lherzolite [72]

In Fig. 14, the panel at left shows experimentally determined solidi, together with a model intraplate geotherm and a mantle adiabat ( $T_p = 1,430$  °C). The intraplate geotherm intersects the mantle dehydration solidus (pargasite-bearing lherzolite) at  $\sim 90$  km, and at deeper levels, a small melt fraction is present if water contents are



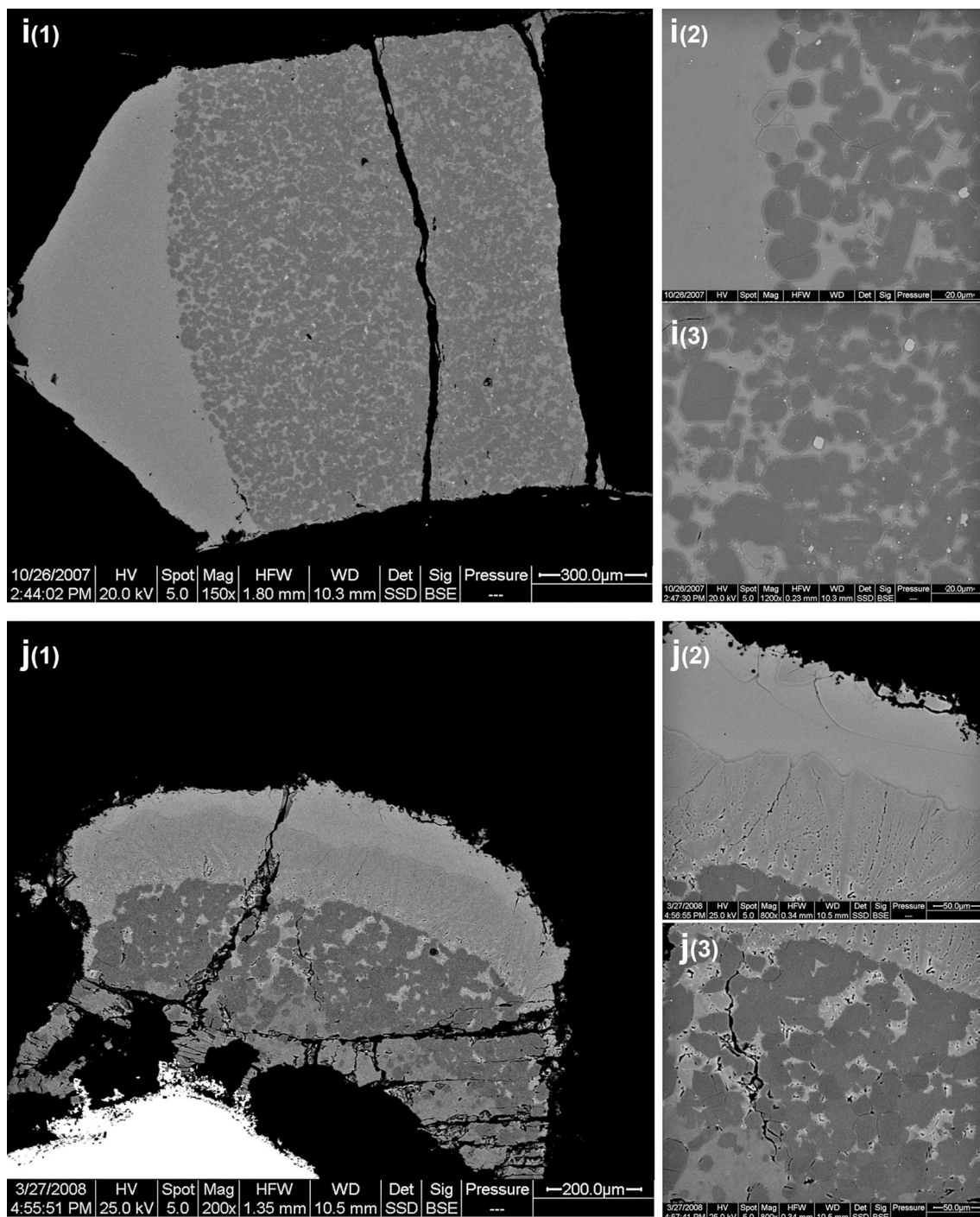
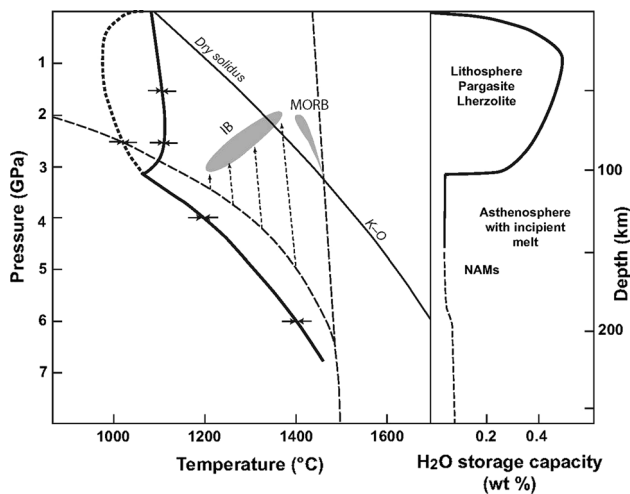


Fig. 13 continued

>200 ppm. The intersection of geotherm and solidus suggests an explanation for the asthenosphere and lithosphere/asthenosphere boundary (LAB). The geotherm is shown joining the mantle adiabat at 200–250 km, and the depth interval from 90 to 250 km is one in which a very small near-solidus melt may migrate along the geotherm, enriching the upper asthenosphere and depleting the lower asthenosphere in incompatible elements. MORB are shown

as sourced from upwelling lower asthenosphere, i.e. a source lherzolite with ~200 ppm H<sub>2</sub>O and depleted LREE and LILE element patterns (Figs. 12a, 14) The melt fraction increases rapidly above the anhydrous solidus, and melt segregation occurs at ~15%–20% melting at ~2 GPa. IB, including OIB, is shown as formed by upwelling of enriched lherzolite from middle and upper asthenosphere, with source water and incompatible element



**Fig. 14** Summary diagram of the results of experiments on fertile lherzolite HZ (Fig. 7 in [51]). Arrows indicate pressures at which the vapour-saturated solidus (hydrous silicate melt) was determined (see text for further discussion)

contents increasing with decreasing depth and decreasing temperature of upwelling (Figs. 12b, 14). Intraplate magmas range from olivine melilitites and nephelinites at deeper levels and smaller melt fraction, to olivine tholeiites with higher melt fraction and higher temperatures (see text; [20, 35, 49, 51]).

The phase relations for fertile or enriched lherzolite compositions such as MPY, HZ or HPY with small H<sub>2</sub>O and carbon (carbonate, graphite, diamond) contents define a distinctive solidus such that the pressure and temperature variations along an intraplate oceanic geotherm pass from subsolidus pargasite-bearing lherzolite (lithosphere) to incipient melt (hydrous, carbonate-bearing silicate melt) in garnet lherzolite (asthenosphere) (Figs. 12, 14, 15). On the basis of the large decrease in strength (viscosity) from subsolidus to incipient melting (~1 %–2 % melt) [76, 78], the base of the lithosphere (LAB) is attributed to the instability of pargasite in lherzolite at >3 GPa and the asthenosphere is interpreted as the underlying depth interval where hydrous silicate melt is present. A model for the lithosphere and asthenosphere based on the experimental studies of lherzolite + C, H, O and of natural parental basaltic magmas is shown in Fig. 15. The importance of the geotherm is illustrated such that the geotherm for intraplate (oceanic or ‘young continental’) locations intersects the (lherzolite + H<sub>2</sub>O + C) solidus at ~90 km, and below this, an interval of incipient melting (carbonate-bearing hydrous silicate melt) extends to 150 km or more. However, a cooler geotherm beneath continental shields may not intersect the silicate melt solidus and will only encounter a carbonatite melt if the local conditions are oxidised ( $fO_2 > IW + 3$  log units).

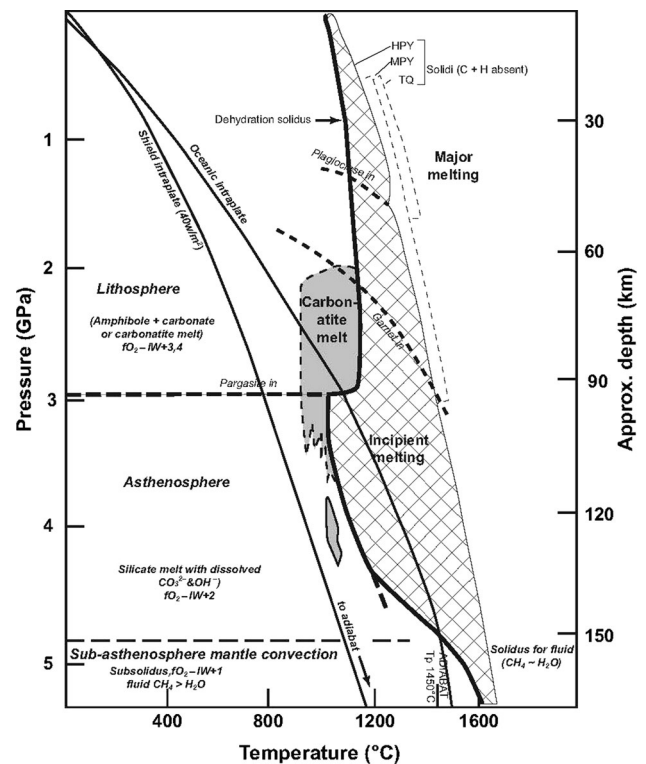


**Fig. 15** A model for the Earth’s uppermost mantle in intraplate locations and emphasising young continent or oceanic crust and lithosphere. The model is based on experimental determination of phase assemblages, solidus and melt compositions of lherzolite and assumes minor carbon and hydrogen (water) in the upper mantle and decreasing oxygen fugacity with increasing depth. A field for carbonatite melt is shown, but it is suggested that this melt is very mobile, even at very small melt fraction and migrates along the geotherm to the decarbonation boundary [70]. Conditions are subsolidus (hydrous silicate melt) to ~90 km defining the lithosphere but at this depth the geotherm enters a  $P, T$  field for incipient melting (the asthenosphere) the melt being a carbonate-bearing olivine + melilitite nephelinite. The presence of 1 %–2 % melt causes a marked decrease in viscosity [76, 78] and a rheological boundary—the LAB. The depth of the LAB is stable against  $T$  variation of ~100 °C due to the steep negative  $dT/dP$  of the pargasite breakdown (dehydration solidus). The lower boundary of the asthenosphere is assumed to be the second intersection of the geotherm and lherzolite solidus which will be dependent on the  $CH_4/H_2O$  of the C, H, O fluid. Slow upward migration of the near-solidus silicate melt within the asthenosphere produces a depth interval of enrichment (upper) and depletion (lower) in incompatible elements, particularly H, C, P, K. Consequently, there is a decoupling of major elements and incompatible trace elements through the asthenosphere. The figure illustrates the argument that the phase relationships and melting behaviour of fertile or enriched lherzolite are a necessary and sufficient condition for the LAB and enable the plate tectonics behaviour of the Earth [49, 51, 73]

### 5.2 Intraplate carbonatite melts

The ubiquitous occurrence of CO<sub>2</sub> fluid inclusions in spinel lherzolite xenoliths, the occurrence of carbonatite magmas, the degassing of CO<sub>2</sub> from both MORB and IB and the presence of diamond or graphite in mantle-derived

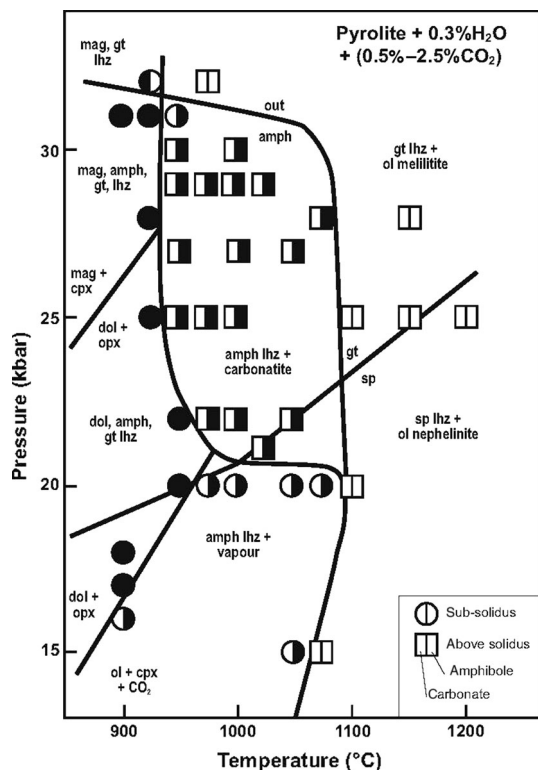


**Fig. 16** Experimental study of melting of enriched lherzolite (HPY) with low H<sub>2</sub>O and CO<sub>2</sub> contents [64]. At low pressure (<2 GPa), a CO<sub>2</sub>-rich vapour phase is present and has little effect on the solidus which is very close to the dehydration solidus for HPY (Figs. 12b, 15). The subsolidus mineralogy is pargasite + spinel lherzolite, and the melt formed at the solidus is a hydrous silicate melt. The carbonation reaction  $Ol + Cpx + CO_2 \rightarrow Dol + Opx$  is intersected with increasing pressure (e.g. at ~1.65 GPa at 900 °C) and garnet replaces aluminous spinel at slightly higher pressure. At 2 GPa, the solidus drops abruptly to ~930 °C at 2.5–3 GPa and the melt formed at the solidus is sodic dolomitic carbonatite in equilibrium with pargasite + garnet lherzolite, i.e. most water remains in pargasite. Pargasite breaks down at higher temperature and melts become transitional from carbonatites through carbonate-rich olivine melilitites to olivine nephelinites. Pargasite is unstable at >3 GPa, and carbonatite melt may occur below the hydrous silicate melt solidus (for example below 1,225 °C at 4 GPa). The carbonatite melt only occurs if  $f_{O_2} \sim FMQ$  or higher and may be accompanied by a water-rich vapour/fluid phase. With increasing temperature, the carbonatite melt dissolves increasing silica and water, but at least in fertile lherzolite such as MPY or HZ there appears to be a distinct solidus between a water-rich vapour/fluid in garnet lherzolite and the appearance of hydrous silicate melt, i.e. normal melting rather than super-critical melting behaviour for MPY and HZ to 6 GPa, as illustrated in Figs. 13 and 14

xenoliths all attest to a significant role for carbon in the Earth's upper mantle [61–63]. In an experimental study of the HPY composition with small water and carbonate contents, Wallace and Green [64] found a *P, T* field where sodic dolomitic carbonatite melt was stable in the presence of pargasite-bearing lherzolite (Fig. 16). The carbonatite field is bounded at low pressures by the decarbonation reactions in which orthopyroxene is consumed producing

olivine and CO<sub>2</sub> vapour. At higher temperatures, approaching and exceeding the water-saturated or dehydration solidi for fertile lherzolite, the carbonatite field passes transitionally into carbonate-bearing hydrous silicate melts. At pressures >3 GPa where pargasite is not stable, carbonatite melt in HPY + H<sub>2</sub>O + CO<sub>2</sub> occurs at temperatures below the vapour-saturated solidus in HPY + H<sub>2</sub>O.

It is now well established by studies of spinel lherzolite suites in IB that decarbonation reactions occur in the lithosphere at ~2 GPa. Ascending sodic-dolomitic carbonatite melts react with lherzolite or harzburgite, releasing CO<sub>2</sub> vapour. Experimental reversal of the reaction was demonstrated by adding CO<sub>2</sub> to a wehrlite (Ol + Cpx + Sp) and a lherzolite at high pressure [65] producing dolomite-bearing pargasite lherzolite or magnesite-bearing pargasite harzburgite, respectively, at 2.2 GPa, 900 °C. The same compositions at 1,000–1,070 °C produced carbonatite melt and at 1,100–1,150 °C yielded carbonate-bearing hydrous silicate melt. In Fig. 15, the model geotherm for oceanic or young continental intraplate locations passes through the solidus (carbonatite melt) of dolomite-bearing pargasite lherzolite at ~2.5 GPa, 920 °C and from the carbonatite to carbonate-bearing hydrous silicate melt field at ~3 GPa, 1,050 °C. The porosity/permeability relationships for carbonatite and carbonate-bearing hydrous silicate melt are not well known, but it is possible that carbonatite melts are very mobile even at very small melt fraction [78]. Their highly fractionated LILE and REE abundances make them effective metasomatic agents, imprinting LREE-enriched patterns on host peridotites. Migration of carbonatite melt along the geotherm in stable regions may produce metasomatised dolomite lherzolite at 70–80 km depth. Upwelling of mantle from the geotherm in the 70–90 km depth interval, if it approaches adiabatic upwelling, will lead to decarbonation reactions, release of CO<sub>2</sub> and metasomatism of lithospheric lherzolite at ~60 km depth. The effects of this process are seen in xenoliths suites from intraplate volcanoes in area of lithospheric stretching and rifting such as SE Australia or New Zealand [23, 65–67] accompanied by an elevated geotherm [68] or local effects of diapirism (Fig. 10).

The definition of a *P, T* field in which sodic, dolomitic carbonatite coexists with residual pargasite-bearing spinel or garnet lherzolite emphasises the sensitivity of incompatible elements to addition or loss of very small melt fractions which are highly enriched, and fractionated (e.g. La/Yb), in LILE and REE [23]. A two-component character was recognised in xenoliths in the SE Australian Newer Volcanics [23]: (1) component A is a residual harzburgite to dunite reflecting variable melt extraction from a 'pyrolite' source. (2) Component B is an added

LREE-enriched melt or fluid of unknown character. Later work clarified the depleted residue character of component A, expressed in major and compatible element compositions [69] and identified component B as access and decarbonation of ephemeral carbonatite melt [64–66, 70]. Owing to the reaction relation between sodic dolomitic carbonatite and orthopyroxene at low pressure, the carbonatite magma cannot ascend by porous flow through the lithosphere at <2 GPa unless it is ‘isolated’ within a dunite or wehrlite channel. In some continental rift environments, there are rare carbonatite magmas which include low-temperature natrocarbonatites (e.g. Oldoinyo Lengai) and dolomitic and calcitic carbonatites—for these magmas, alternative models of liquid immiscibility from carbonate-bearing silicate magmas at crustal pressures, or direct melting of lherzolite + H<sub>2</sub>O + CO<sub>2</sub> are debated. The experimentally determined compositions of the sodic dolomitic carbonatite melts in HPY [64], reconstructed from natural wehrlite and harzburgite xenoliths [65] and equilibrated with residual peridotites [71] do not resemble the Oldoinyo Lengai lavas, i.e. these experimental studies do not support a direct mantle melting model for Oldoinyo Lengai natrocarbonatites.

## 6 Intraplate versus mid-ocean ridge magmatism: ‘hot-spots’ or not

To summarise the previous discussion of intraplate volcanism, the spectrum of parental mantle-derived mafic magmas from carbonate-bearing olivine melilitite to olivine tholeiite are derived by (H<sub>2</sub>O + CO<sub>2</sub>)-fluxed melting of upwelling lherzolite from the asthenosphere. The spectrum of increasing silica saturation correlates with increasing melt fraction and decreasing pressure, magmas separating from residual garnet lherzolite through spinel lherzolite to harzburgite at decreasing pressure from ~3 to ~1.5 GPa. The lowest melt fractions are also the most enriched in incompatible elements, including (H<sub>2</sub>O + CO<sub>2</sub>). The relative abundances of REE particularly argue that both garnet and clinopyroxene are residual phases at least for magmas from olivine melilitites to olivine-rich basanites. The intraplate magmas which are hottest and largest melt fraction are the olivine tholeiites and tholeiitic picrites, particularly from island chains, or shield volcanoes on continental crust (‘hot-spots’). For these primary magmas, residual phases at segregation from the upper mantle are olivine, orthopyroxene and Cr-rich spinel (clinopyroxene-free harzburgite). The characteristics of some primary ‘hot-spot’ magmas are summarised in Table 1 based particularly on the Hawaiian volcanoes (see also Table 1 in [21], Table 2 in [20] and Table 5 in [25]). Parental magmas have 14 wt%–17 wt% MgO, liquidus

olivine microphenocrysts with Mg# = 89–91.5, spinel with Cr# = 60–75 and liquidus temperatures of 1,290–1,370 °C (including liquidus depression by ~0.6 wt%–0.7 wt% H<sub>2</sub>O and CO<sub>2</sub>). The parental magmas are extracted from residual harzburgite with Cr-rich spinel and without clinopyroxene at 1.5–2.5 GPa. The source peridotites are complex and inhomogeneous including high and low CaO/Al<sub>2</sub>O<sub>3</sub> relative to MOR picrite sources. They are enriched and variable in incompatible elements and isotopic ratios and inferred to have experienced both melt extraction and refertilisations with low-degree near-solidus melts at high pressure. Estimation of melt fraction is dependent on assumed source composition, i.e. 20 %–30 % melt if an enriched lherzolite such as HPY is assumed, but 10 %–15 % melt if the sources were refertilised harzburgite with minor clinopyroxene + spinel.

In comparison with MORB, these ‘hot-spot’ magmas or OIB are enriched in LILE and in LREE relative to HREE. As the separation of tholeiitic picrite from residual harzburgite does not cause fractionation among incompatible elements, their sources must have been enriched prior to or during upwelling and prior to the melt segregation process.

Referring to the previous discussion of MORB, the study of glasses and phenocrysts argues for parental magmas which are also tholeiitic picrite, segregating from residual lherzolite to harzburgite at pressures of 1.5–2 GPa. Although the melt fraction for some parental magmas is such that some clinopyroxene remains as a residual phase (lherzolite transitional to harzburgite), the observed low abundances of LILE, and the LREE-depletion must be attributed to the source, i.e. prior loss of a very small melt fraction from garnet lherzolite. The large majority of MORB glass compositions is not primary melts from lherzolithic mantle but exhibits effects of crystal fractionation (low Mg# of glass), multiphase saturation (olivine, spinel, plagioclase, clinopyroxene) and/or magma mixing (xenocrysts of anorthitic plagioclase). However, glasses with >9.5 wt% MgO occur among MORB and are saturated at low pressure in olivine and spinel (Cr# = 20–50). They may contain microphenocrysts of olivine with core compositions of Mg# >90 which is higher than the liquidus olivine for the glass. Incremental addition of equilibrium olivine is valid up to the Mg# of the observed microphenocrysts in order to calculate the most primitive (parental, primary) mantle-derived magma. This approach identifies MOR parental magmas as picrites with 13 wt%–16 wt% MgO, liquidus olivine with Mg# = 89–91.5 and liquidus temperature of 1,240–1,360 °C (including the effect of 0.1 wt%–0.3 wt% H<sub>2</sub>O and CO<sub>2</sub>) (Table 1). The parental magmas are extracted from residual harzburgite with minor subcalcic clinopyroxene and Cr–Al spinel at 1.5–2 GPa. They represent a melt fraction of 15 %–25 % from a fertile

lherzolite such as MPY or HZ (including  $\text{CaO}/\text{Al}_2\text{O}_3 \sim 0.8$ ).

The preceding discussion argues that *there is no significant difference in the eruption temperatures of the primary picrites of ‘hot-spot’ and MOR locations*. The harzburgite residue and higher Cr# of spinel for ‘hot-spot’ picrites rather than lherzolite–harzburgite residue and low Cr# of spinel for MOR picrites are a consequence of higher ( $\text{H}_2\text{O} + \text{CO}_2$ ) and different source composition, rather than higher temperature in the ‘hot-spot’ source. The lherzolite to harzburgite residue and relatively low Cr# of spinel inferred for parental MORB apply to a ‘fertile’ lherzolite source such as MPY or HZ (i.e. an estimate of modern well-mixed mantle). If the ‘hot-spot’ source was an ‘enriched’ lherzolite source such as HPY, then the harzburgite residues inferred would require a larger melt fraction for parental ‘hot-spot’ picrites than for MOR picrites. However, we argue that the ‘hot-spot’ source was

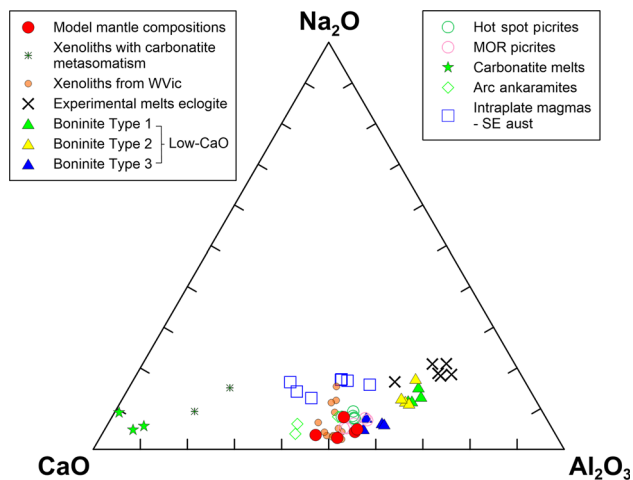


**Fig. 17** (Color online) Triangular plot showing relationships between three oxides ( $\text{CaO}$ ,  $\text{Na}_2\text{O}$ ,  $\text{Al}_2\text{O}_3$ ) in lherzolitic mantle (model compositions), primary magmas, a mantle xenolith suite and contrasted ‘refertilising melts’ (carbonatites, olivine melilitites and rhyodacites). The sources, residues and melts for high-degree melting (tholeiitic picrites, picritic alkali olivine basalts) at spreading centres and ‘hot-spots’ show little change in  $\text{Ca}/\text{Al}$  and magmas and residues are enriched and depleted respectively in  $\text{Na}_2\text{O}$  by magma extraction. By contrast, sodic dolomitic carbonatite has very low  $\text{Al}$  and metasomatism in the lithosphere by decarbonation reactions causes marked shifts in compositions as demonstrated by xenolith suites [23, 66, 67, 69, 70]. The position of parental ‘arc ankaramites’ and the experimental study of the effects of  $\text{CO}_2$  and  $\text{H}_2\text{O}$  on arc ankaramite have led to suggestions of a role for carbonatite melt in the mantle wedge above some subduction zones [35, 60, 74]. It is also argued that hydrous dacitic–rhyodacitic (adakitic) magmas derived from melting of eclogite (subducted mafic crust) can ascend into the mantle wedge, fluxing melting of residual to refractory peridotite. The high  $\text{Al}/\text{Ca}$  and  $\text{Na}/\text{Ca}$  of adakitic melts mix with the  $\text{Na}$ ,  $\text{Ca}$ ,  $\text{Al}$  of wedge peridotite and are most clearly seen in the low- $\text{Ca}$  boninites for which the wedge peridotite is inferred to be particularly refractory, i.e. clinopyroxene-free harzburgite for types 1 and 2 Lo- $\text{Ca}$  boninite [74, 75]

more complex, with a bulk composition of depleted to refractory lherzolite to harzburgite, i.e. recycled mantle with 1 %–3 %  $\text{CaO}$  and  $\text{Al}_2\text{O}_3$ , but refertilised at high pressure by very small melt fraction(s), including near-solidus melts from garnet lherzolite and reactive rhyodacite melts from old subducted crust (Figs. 17, 18).

In Fig. 15a, b, models for genesis of MOR picrites and intraplate magmas are illustrated, integrating the studies of melting of lherzolite + ( $\text{C}$ ,  $\text{H}$ ,  $\text{O}$ ) and the effects of ( $\text{H}_2\text{O} + \text{CO}_2$ ) on the liquidus temperatures and phases of olivine-rich magmas. Two examples differing in water and carbon content are illustrated, both with mantle adiabat of  $T_p = 1,430^\circ\text{C}$  and Fig. 15a representing MORB source. The contour for  $\sim 2\%$  melt is shown marking where melt is assumed to segregate within the buoyant upwelling. The experimental study of water in NAMs and the Lherzolite +  $\text{H}_2\text{O}$  solidus [51, 58, 59] established that  $\sim 200$  ppm  $\text{H}_2\text{O}$  remains in NAMs at the vapour-saturated solidus at 2.5–4 GPa and the hydrous silicate melt at the solidus has  $\sim 30$  wt%  $\text{H}_2\text{O}$ . Upwelling from the deeper asthenosphere crosses contours of incipient melting until close to the anhydrous solidus where melt fraction rapidly increases, the  $P$ ,  $T$ , path departs from the olivine adiabat due to latent heat of melting and melt segregates into dunite channels/dykes breaking out of the diapir at  $\sim 2$  GPa,  $1,400^\circ\text{C}$ , 15 %–25 % melting.

In Fig. 15b, higher ( $\text{H}_2\text{O} + \text{CO}_2$ ) contents are assumed so that the 2 % melting contour is at much lower temperature. The inferred depths of melt segregation for primitive and mantle xenolith-bearing basalts from SE Australia are shown [52]. In Fig. 15a, b, intraplate (including ‘hot-spot’) magmas are inferred to have similar or lower temperatures and depths of magma segregation when compared with those of MOR picrites, but the source compositions differ in incompatible elements, particularly in ( $\text{H}_2\text{O} + \text{CO}_2$ ). It is suggested that these differences arise in intraplate locations because the asthenosphere is a region of chemical differentiation rather than a region of homogenisation. The incipient melt fraction in the asthenosphere, illustrated by the geotherm of Fig. 15a, b being subparallel to the % melt contours, migrates slowly (relative to plate movement) upward so that the base of the asthenosphere becomes depleted (Fig. 15a) and the upper asthenosphere becomes enriched (Fig. 15b) in incompatible elements. The migrating incipient hydrous silicate melt is trapped below  $\sim 90$  km as any further penetration results in pargasite  $\pm$  phlogopite crystallisation at the base of the lithosphere. In the initial stages of new rifting of a plate, the process of lithospheric thinning and asthenospheric upwelling samples the upper, enriched asthenosphere and base of the lithosphere (pargasite-enriched) and only after some time is the depleted lower asthenosphere drawn into the mature MOR magmatism (see figs. in [49]).

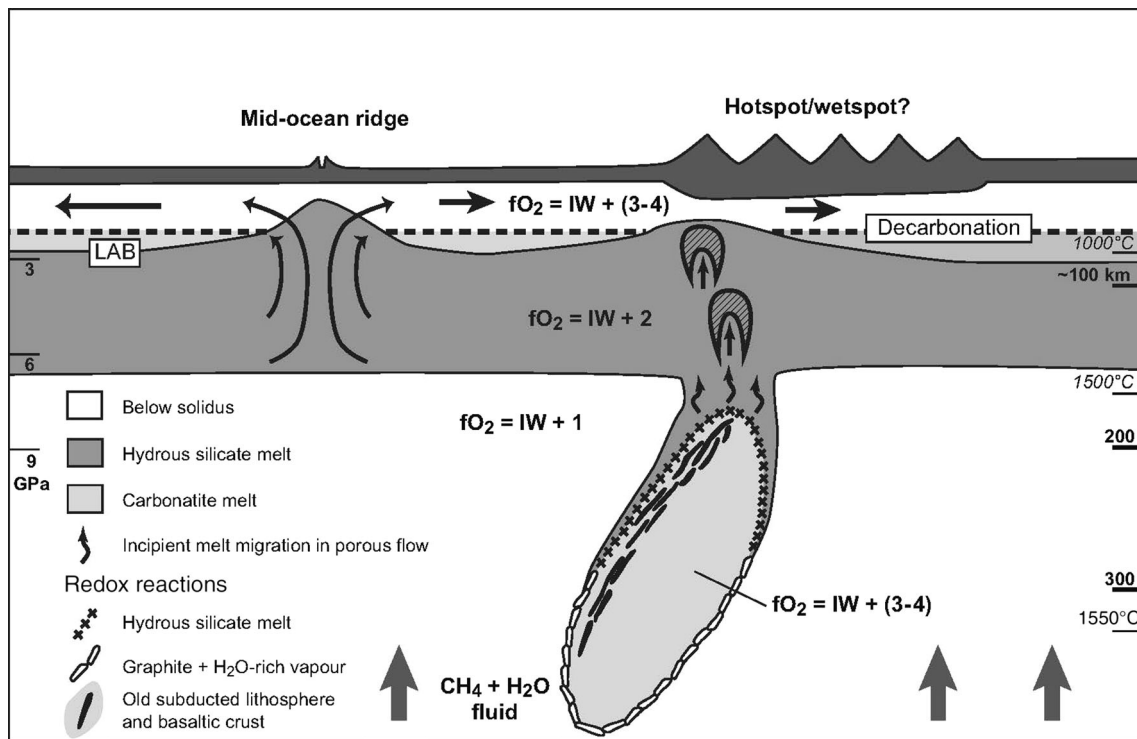


**Fig. 18** Diagram suggesting a model for intraplate ‘hot-spot’ or island chain volcanism, in which the cause of the volcanism is ‘fixed’ relative to lithospheric plate movement. The model attributes the cause of the long-lived melting anomaly to compositional heterogeneity within the mantle beneath or within the lowermost part of the asthenosphere. Specifically, the compositional heterogeneity is suggested to be old subducted slab(s) and the interface between such slabs and ambient mantle is a redox contrast at which  $f_{H_2O}$  is a maximum, triggering melting at the water-saturated solidus or (at deeper levels) graphite/diamond and water-rich fluid. The near-solidus melts are depicted as lowering viscosity to permit diapirism in which mixing and reaction occurs between asthenospheric mantle and old subducted crust + lithosphere. Melt segregation within upwelling mantle occurs at shallower depths and higher melt fraction. Although the model suggests a temperature anomaly (‘plume’) at shallow depths in lithosphere and asthenosphere, there is no deep-seated thermal plume and the melting anomaly is effectively due to higher (C, H, O) contents and chemical heterogeneity of the old subducted slab/ambient mantle interface (reproduced from [73], see also [35])

We consider that the argument for a chemically zoned asthenosphere based on the phase relations of lherzolite + (C, H, O) offers an explanation for intraplate volcanism exemplified by rifts, continental basaltic provinces such as SE Australia and isolated seamounts (including ‘petit-spots’ [4]). However, the island chains or ‘hot-spots’, although having similarly enriched incompatible element contents, produce high magma fluxes and are episodic but enduring magma sources. From isotopic, trace element and major element (e.g. Ca/Al) data, the ‘hot-spot’ sources are heterogeneous and provide evidence for admixture of older oceanic and continental crust. Higher incompatible element contents and fractionated relative abundances suggest small melt fractions and garnet lherzolite residues. This is contradicted by major element compositions, particularly of compatible and refractory elements, which suggest refractory harzburgite residues, i.e. very large melt fraction or a previously depleted source. A more refractory nature of ‘hot-spot’ sources is indicated by more Cr-rich spinels in Hawaiian picrites than in MOR picrites. Reconciling these

indicators suggests that the detachment between incompatible element abundances and fractionation, and the major and compatible element compositions, is a consequence of mobility of near-solidus melts. An additional process is the recycling in intraplate settings of old subducted slabs in which refractory lithosphere has been refertilised by incompatible element-enriched fluids or melts. Different mechanisms for such enrichments have been suggested and can be explored by relationships among Ca, Al and Na—the three major elements with no or low solubility in olivine and orthopyroxene. For example, variation of Ca/Al (Fig. 17) may be caused by refertilisation of harzburgite by reaction with rhyodacitic to dacitic (adakitic) melts from subducted eclogite (low Ca/Al) or by sodic, dolomitic carbonatite from incipient melting of lherzolite + C, H, O (high Ca/Al). The slightly incompatible to compatible oxides  $Na_2O$ , CaO and  $Al_2O_3$  differ in their relative melt/residue partitioning as residues vary from fertile lherzolite to harzburgite or dunite. In Fig. 17, the model mantle compositions MPY, HZ, HPY overlap

the tholeiitic picrites of MOR and ‘hot-spots’, i.e. there is little fractionation among these three elements for high melt fractions (contrasting with the variability of highly incompatible elements, LREE and LILE, between and within each of these groups). The primary intraplate magmas such as xenolith-bearing olivine-rich basanite to olivine nephelinite to olivine melilitite from SE Australia are relatively enriched in  $\text{Na}_2\text{O}$ , and the most undersaturated magmas show enrichment of CaO relative to  $\text{Al}_2\text{O}_3$ . The mantle xenolith suites have been investigated by several authors, and we illustrate the sequence from harzburgite to fertile lherzolite [23, 69] which provides evidence for inefficient tholeiitic picrite melt extraction [69] from enriched lherzolite similar to HPY, followed by reaction of harzburgite to lherzolite residues with sodic, dolomitic carbonatite melt at the decarbonation boundary ( $\sim 2$  GPa [23]). The positions of two xenoliths (asterisks) in which the carbonatite metasomatism was experimentally reversed [65] to convert natural wehrlites (+ $\text{CO}_2$ ) to lherzolite + sodic dolomitic carbonatite demonstrate the local effect of  $\sim 10$  wt% carbonatite melt on lithospheric mantle and are well illustrated in this simple figure. The compositions of carbonatite melts derived by experiments at  $\sim 2.2$  GPa 1,000–1,100 °C [64, 65] are shown (green stars). Among the intraplate primary magmas, the positions of the olivine melilitites and olivine nephelinites suggest a carbonatitic component and enriched lherzolite source.

Attention is drawn to the arc ankaramites (green diamonds), exemplified by parental magmas from Vanuatu island arc [74, 77, 79]. In these magmas, the fluxing of melting in depleted lherzolite or harzburgite by carbonatite melt + water-rich fluid in the mantle wedge environment has been suggested, based on experimental studies [79]. Some island arc settings also have distinctive boninite magmas with high MgO and Mg#, high  $\text{SiO}_2$  and extremely refractory chromite (Cr# = 80–90). CaO and  $\text{Na}_2\text{O}$  are variable, recognised in Types 1, 2 and 3 of the low-Ca boninites and the high-Ca boninites [75]. In this diagram, the high-Ca boninites (not plotted) overlap the depleted lherzolites to harzburgites, i.e. have  $\text{CaO}/\text{Al}_2\text{O}_3 \sim 0.8$  and low  $\text{Na}_2\text{O}$  contents. In compatible element and phase equilibria respects, these magmas are consistent with fluxing of melting by water-rich fluid entering depleted lherzolite of the mantle wedge above the subducting crust and lithosphere. However, the trend of increasing  $\text{Na}_2\text{O}$  and decreasing  $\text{CaO}/\text{Al}_2\text{O}_3$  from Type 3 to Type 1 of the low-Ca boninites cannot be attributed to addition of water-rich fluids (dilute solutions of Na, Al, Ca, Si, etc.) but is consistent with hydrous adakitic (‘dacite–rhyodacite’) melts derived by melting of subducted eclogite or garnet amphibolite in the upper part of subducted oceanic crust and lithosphere. In Fig. 17, the low-Ca boninite trend leads to the compositions of melts derived from quartz/coesite

eclogite and probably reflects the potential range of mantle wedge peridotite (harzburgite–lherzolite) together with the invasive melt fraction. If this model of low-CaO boninite genesis is correct, then the  $\text{H}_2\text{O}/\text{Na}_2\text{O}$  of the boninite reproduces the  $\text{H}_2\text{O}/\text{Na}_2\text{O}$  of the slab melt. Melting is water undersaturated, and ratios among highly incompatible elements are those of the fluxing melt rather than the refractory mantle wedge.

The preceding brief discussion of the further complexity of mantle-derived magmas in island arcs is the basis for our preferred model for intraplate, ‘hot-spot’ magmatism. Figure 18 is a cartoon, suggesting that rather than deep-seated high-temperature mantle plumes carrying recycled subducted crust and lithosphere from the CMB, ‘hot-spot’ sources are embedded in the upper mantle. Melting is localised at the interface between recycled subducted crust and lithosphere occurring as neutrally buoyant or positively buoyant slabs embedded in or below the lower part of the asthenosphere. The upwelling and decompression melting responsible for ‘hot-spot’ volcanism is explained by compositional difference rather than by a thermal anomaly attributed to a deep mantle plume. In the formation of oceanic crust and residual lithosphere at mid-ocean ridges, the residual lithosphere has higher Mg# than asthenospheric mantle (MPY, HZ) and is lower in Ca, Al, Ti and Na [80]. Residual lithosphere is negatively buoyant (subduction) only because it is ‘cold’. Basaltic crust only becomes negatively buoyant after dehydration and reaction to eclogite during subduction. Also, subduction is accompanied by melting in the mantle wedge overlying the subducted slab (fluxed by fluid/melt from the slab), and the residue from hydrous melting of depleted and refertilised lithosphere (1 %–3 % CaO,  $\text{Al}_2\text{O}_3$ ) is refractory harzburgite (<1 % CaO,  $\text{Al}_2\text{O}_3$ ) of high Mg#  $\sim 92$ –93 and minor chromite (Cr#  $\sim 80$ ). Incorporation of this residue by subductive erosion of fore-arc crust and lithosphere may recycle potentially buoyant harzburgite which is chemically heterogeneous and complex in isotopic and incompatible trace element compositions. Most importantly, the subducted slab with a mix of lithologies all experiencing surface or near-surface  $P$ ,  $T$  conditions is oxidised, particularly carrying high  $\text{Fe}^{3+}/(\text{Fe}^{2+} + \text{Fe}^{3+})$  and carbonate/carbonatite melt. The interface or mixing zone between ambient asthenospheric or subasthenospheric mantle and an embedded old subducted slab will be a redox front, in which high  $f\text{O}_2$  will be accompanied by high  $f\text{H}_2\text{O}$  and lead to incipient melting in the peridotite + ( $\text{CO}_2 + \text{H}_2\text{O}$ ) system.

## 7 Summary

The paper summarises related experimental high-pressure/high-temperature studies on magma compositions which,

on the basis of compatible element contents and other evidence such as transport of mantle-derived xenoliths, are inferred to be possible partial melts formed in the upper mantle and are parental to other evolved melts by shallow crust or uppermost mantle crystal fractionation. Parental or primary magmas from mid-ocean ridge, intraplate and ‘hot-spot’ or ‘island chain’ settings have been identified on the basis of experimentally determining the  $P$ ,  $T$  conditions for olivine, orthopyroxene, Cr–Al spinel  $\pm$  clinopyroxene as liquidus phases. The second constraint used is that of liquidus olivine Mg#  $\sim 90$ , i.e. matching that of upper mantle lherzolite samples. We have focussed on the oft-quoted hypothesis that intraplate volcanism leading to ‘island chains’ is a consequence of thermal plumes arising from the CMB where cold subducted slabs are assumed to accumulate. An essential characteristic of this hypothesis is that there is a temperature difference of  $\sim 200$  °C or more between upwelling plume from the CMB generating ‘hot-spot’ basalts, and ambient mantle generating MORB. This has been tested.

Parental magmas in MOR settings are picrites separating from residual (clinopyroxene + Al-rich spinel)-bearing harzburgites at pressures of 1.5–2 GPa and temperatures of  $\sim 1,400$  °C and at 15 %–25 % melting assuming a lherzolite source with 3 wt%–4 wt% CaO and Al<sub>2</sub>O<sub>3</sub> (CaO/Al<sub>2</sub>O<sub>3</sub>  $\sim 0.8$ ). This conclusion is based on major element and compatible element compositions. Incompatible element contents (including H, C) of both sources and parental magmas show depleted (N-MORB) to refractory (D-MORB) LILE and LREE abundances and patterns, or less common slightly enriched (E-MORB) patterns. The inferred source composition is lherzolite which has lost a (H<sub>2</sub>O > CO<sub>2</sub>)-rich incipient melt (near the vapour-saturated solidus) in the garnet lherzolite stability field.

Parental magmas in ‘hot-spot’ settings are also picrites separating from residual harzburgite at pressures of 1.5–2.5 GPa and temperatures of  $\sim 1,450$  °C (anhydrous) but lowered to  $\sim 1,370$  °C by water contents of 0.5 wt%–1 wt% H<sub>2</sub>O and small CO<sub>2</sub> contents in the magmas. This conclusion is based on major and compatible element compositions. There is a significant difference between MOR and ‘hot-spot’ picrites in that the latter have olivine + orthopyroxene + Cr-rich spinel as liquidus phases at high pressure. Compositions from a single volcano plot on Ol + Opx control lines, consistent with more refractory residues (Cpx-free) than that from MOR picrites. Individual volcanoes also show different Ca/Al, Ti/Al, Fe/Mg ratios suggesting major element heterogeneity among sources. Incompatible element contents (including H, C) of parental magmas show enriched LILE, P and LREE abundances and patterns. The estimation of melt fraction is dependent on the assumed source, i.e. if lherzolite with 3 wt%–4 wt% CaO and Al<sub>2</sub>O<sub>3</sub> is correct, then tholeiitic

picrites require up to 30 %–35 % melting to yield Cpx-free residue with Cr-rich spinel. However, if the source composition (major elements and compatible trace elements) is depleted lherzolite to harzburgite with 1 wt%–2 wt% CaO and Al<sub>2</sub>O<sub>3</sub>, then the melt fraction is lower, around 15 %–20 %.

In intraplate settings such as rifts, fracture zones or sea floor ‘petit-spots’, mantle-derived parental magmas from alkali olivine basalts to olivine nephelinites, olivine melilitites and lamprophyres can be selected on the basis of transport of dense mantle xenoliths and liquidus olivine with Mg#  $\sim 90$ . Incompatible elements LILE, P and LREE are enriched and increasingly fractionated. Both H<sub>2</sub>O and CO<sub>2</sub> are enriched and correlate with increasing silica undersaturation. Experimental studies at variable  $P$ ,  $T$ , H<sub>2</sub>O and CO<sub>2</sub> contents established conditions for Ol + Opx + Cpx  $\pm$  Ga or Sp as liquidus phases with  $P$  increasing and both  $T$  and melt fraction decreasing in the continuum from olivine tholeiites, through alkali olivine basalts, olivine-rich basanites, olivine nephelinites to olivine melilitites.

We consider that the sources of parental magmas in MOR, intraplate and ‘hot-spot’ settings are characterised by two components, the major element and compatible element compositions (A) which vary from ‘fertile lherzolite’ (asthenospheric or MORB source composition such as MPY or HZ) to refractory harzburgite [80]. A second component (B), which dominates incompatible element contents (including H, C, P and S) and related isotopic ratios, is near-solidus melt in garnet lherzolite, close to the vapour-saturated solidus for carbon-bearing lherzolite + H<sub>2</sub>O. Component B may be sodic, dolomitic carbonatite or carbonate-bearing hydrous nephelinitic or melilitite. From the companion studies of melting of lherzolite + (C, H, O), we argue that the asthenosphere becomes chemically zoned, the deeper asthenosphere is depleted by loss of incipient melt (component B) and the upper asthenosphere is enriched by upward percolation of this melt. Additional heterogeneity in the upper mantle is suggested for ‘hot-spot’ or ‘island chain’ sources—this heterogeneity may be thermal, required for the deep mantle plume hypothesis, or compositional. We note the following compositional effects on density ( $\rho$ ) at a given pressure:  $\Delta\rho = 0.02$  gm/cc for olivine Mg# varying from 90 to 92;  $\Delta\rho = 0.06$  gm/cc for fertile garnet lherzolite (3 wt%–4 wt% CaO and Al<sub>2</sub>O<sub>3</sub>) to refractory ophiolitic harzburgite (<0.5 wt% CaO and Al<sub>2</sub>O<sub>3</sub>). A density difference of ( $\Delta\rho = 0.02$ ) requires  $\Delta T \sim 200$  °C if the density difference between plume or diapir and ambient mantle is attributed to temperature heterogeneity rather than compositional heterogeneity. It is highly probable that subducted slabs with significant contents of refractory harzburgite become neutrally or positively buoyant in the

upper mantle as temperatures rise. Similarly, delamination of deep cratonic lithosphere of refractory composition may create buoyant volumes within ‘modern well-mixed mantle’ of MPY or HZ composition.

Experimental study of parental melts from MOR and ‘hot-spot’ demonstrates that there is no significant difference between eruption temperatures or  $P$ ,  $T$  conditions of magma segregation from residual peridotite. There is variation of  $\pm 30$  °C between parental magmas in both settings, but there is not excess temperature of  $\sim 200$  °C beneath ‘hot-spot’ volcanoes as required by the ‘deep mantle thermal plume’ hypothesis [2, 5, 7]. From our own studies and arguments summarised in Foulger [5], we infer that the causes/sources for ‘hot-spot’ magmas: (1) are not fixed, but their relative movements are slower and unrelated to lithospheric plate motion; (2) have higher (C, H, O) volatiles than MOR sources; (3) leave more refractory residue (harzburgite: Ol + Opx + Cr spinel) than those from MORB extraction; (4) have higher and more fractionated incompatible element abundances, including residual ‘garnet signature’, and heterogeneity (including isotopes); (5) have heterogeneity in Ca/Al, Ti/Al and Fe/Mg; (6) have parental picrite magmas with eruption temperatures similar to parental MOR picrites; and (7) cause a thermal anomaly in the lithosphere.

The causes of ‘hot-spot’ volcanism lie within or below the asthenosphere and do not move with lithospheric plates. The upper mantle is inhomogeneous in composition and includes neutrally or positively buoyant bodies formed as more refractory residues of old subducted slabs or from delaminated cratonic lithosphere. Because a redox contrast between relatively oxidised subducted crust and lithosphere [carbonate, high  $\text{Fe}^{3+}/(\text{Fe}^{2+} + \text{Fe}^{3+})$ ] will maximise water activity at the interface, we suggest that ‘hot-spot’ sources are from melting and diapirism at interfaces between ‘old slab’ and MORB source mantle (Fig. 18). We concur with other investigators (summarised in [5]) that plate tectonics is driven by surface cooling and lithospheric subduction and that there is no evidence from mantle-derived magmas (as the indicators for mantle temperature) for additional independent thermal plumes from deep mantle or CMB.

**Acknowledgments** The lecture on which this paper is based was given to honour the memory of Dr. Shensu Sun, his contributions to geochemistry and his support of international collaborations and to the careers of young scientists. It was given at the annual Chinese Conference on Geochemistry and Geodynamics held at Lanzhou University in 2012. Green D H most warmly thanks Professors Yaoling Niu and Weidong Sun for their friendship, organisation, care and generosity of time during this visit. The generous hosting by colleagues at the Chinese Academy of Sciences in Beijing, Chinese University of Geosciences, Peking University, Lanzhou University, Northwestern University in Xi’an, Nanjing University and Chinese Academy of Sciences in Guangzhou is greatly appreciated. Ms. Fengli

Shao and Ms. Yan Hu were excellent guides and facilitators throughout and helped to make a memorable visit. The visit also followed the presentation of the IMA Medal lecture at the European Mineralogical Societies Conference in Frankfurt, Germany, using much of the same material. The lectures summarised sequential and related research on the petrology of the Earth’s Upper Mantle, with emphasis on melting and the importance of small water and carbon contents. The contents were largely drawn from high-pressure experimental investigations carried out at University of Tasmania and the Australian National University from 1962 to 2012, by the authors, research fellows, Ph.D. students and visitors, and with excellent technical and professional support. Many of these contributors are named in the references, and we acknowledge their contributions and teamwork, and the support of the Department of Geology/School of Earth Sciences at University of Tasmania and the Research School of Earth Sciences, Australian National University. The Australian Research Grants Committee/Australian Research Council and the Australian National University were major sources of funding for the research which enabled the continuity of a coherent and interactive programme. At University of Tasmania, ‘Earth Sciences’ and ‘Centre for Ore Deposits and Exploration Studies (CODES)’ are thanked for support for the preparation of this paper. The expansion from lectures to publication resulted in two papers with some overlap and reuse of illustrations: (1) the IMA lecture [73] emphasised the ‘forward’ approach to magma genesis, i.e. subsolidus phase relations and melting of peridotite, (2) this paper which emphasises the ‘inverse’ approach, i.e. the high pressure liquidus phases of mantle-derived magmas, their liquidus temperatures and solution of volatiles, particularly water and carbonate. A common theme throughout these experimental studies was also the parallel study of the petrology and geochemistry (major, minor and trace elements) of natural peridotites, eclogites, mantle xenoliths and mantle-derived parental and derivative magmas.

**Conflict of interest** The authors declare that they have no conflict of interest.

## References

1. Niu Y, Batiza R (1991) An empirical method for calculating melt compositions produced beneath mid-ocean ridges: application for axis and off-axis (seamounts) melting. *J Geophys Res* 96:21753–21777
2. Davies GF (1998) Plates, plumes, mantle convection and mantle evolution. In: Jackson INS (ed) *The Earth’s mantle: composition, structure and evolution*. Cambridge University Press, Cambridge, pp 228–258
3. Campbell IH, Davies GF (2005) Do mantle plumes exist? *Episodes* 29:162–168
4. Hirano N, Takahashi E, Yamamoto J et al (2006) Volcanism in response to plate flexure. *Science* 313:1426–1428
5. Foulger GR (2010) *Plates vs plumes: a geological controversy*. Wiley, Oxford, pp 1–328
6. McKenzie DB, Bickle MJ (1988) The volume and composition of melt generated by extension of the lithosphere. *J Petrol* 29:629–679
7. Campbell IH, Griffiths RW (2005) Implications of mantle plume structure for the evolution of flood basalts. *Earth Planet Sci Lett* 99:79–93
8. Engel AEJ, Engel CG, Havens RG (1965) Chemical characteristics of oceanic basalts and the upper mantle. *Geol Soc Am Bull* 76:719–734
9. Chalot-Prat F, Falloon TJ, Green DH et al (2010) An experimental study of liquid compositions in equilibrium with

- plagioclase + spinel lherzolite at low pressures (0.75 GPa). *J Petrol* 51:2349–2376
10. Chalot-Prat F, Falloon TJ, Green DH et al (2013) Melting of plagioclase + spinel lherzolite at low pressures (0.5 GPa): an experimental approach to the evolution of basaltic melt during mantle re-fertilisation at shallow depths. *Lithos* 172–173:61–80
  11. Ballhaus C, Berry RF, Green DH (1990) Oxygen fugacity controls in the Earth's upper mantle. *Nature* 348:437–440
  12. O'Neill HSC, Wall VJ (1987) The olivine–orthopyroxene–spinel oxygen barometer, the nickel precipitation curve and the oxygen fugacity of the upper mantle. *J Petrol* 28:1169–1191
  13. Gupta AK, Green DH, Taylor WR (1987) The liquidus surface of the system forsterite–nepheline–silica at 28 kb. *Am J Sci* 287:560–565
  14. Taylor WR, Green DH (1987) The petrogenetic role of methane: effect on liquidus phase relations and the solubility mechanism of reduced C–H volatiles. In: Mysen BO (ed) *Magmatic processes and physicochemical principles*. Geochem. Soc. Spec. Publ. No. 1, Pennsylvania State University, University Park, Pennsylvania, pp 121–138
  15. Green DH, Falloon TJ, Taylor WR (1987) Mantle-derived magmas—roles of variable source peridotite and variable C–H–O fluid compositions. In: Mysen BO (ed) *Magmatic processes and physicochemical principles*. Geochem. Soc. Spec. Publ. No. 1, Pennsylvania State University, University Park, Pennsylvania, pp 139–154
  16. Taylor WR, Green DH (1988) Measurement of reduced peridotite–C–O–H solidus and implications for redox melting of the mantle. *Nature* 332:239–352
  17. Odling NWA, Green DH, Harte B (1997) The determination of partial melt compositions of peridotitic systems by melt inclusion synthesis. *Contrib Mineral Petrol* 129:209–221
  18. Falloon TJ, Green DH, Hatton CJ et al (1988) Anhydrous partial melting of fertile and depleted peridotite from 2 to 30 kbar and application to basalt petrogenesis. *J Petrol* 29:257–282
  19. Green DH (1976) Experimental testing of 'equilibrium' partial melting of peridotite under water-saturated, high pressure conditions. *Can Mineral* 14:255–268
  20. Green DH, Falloon TJ (2005) Primary magmas at mid-ocean ridges, "hotspots", and other intraplate settings: constraints on mantle potential temperature. In: Foulger G, Natland J, Presnall D et al (eds) *Plates, plumes and paradigms*. Geological Society of America Special Paper 388, Boulder, CO, pp 217–247
  21. Green DH, Falloon TJ, Eggins SM et al (2001) Primary magmas and mantle temperatures. *Eur J Mineral* 13:437–451
  22. Danushevsky LV, Plechov P (2011) Petrolog3: integrated software for modelling crystallization processes. *Geochem Geophys Geosyst* (G3) 12:1–32. doi:10.1029/2011GC003516
  23. Frey FA, Green DH (1974) The mineralogy, geochemistry and origin of lherzolite inclusions in Victorian basanites. *Geochim Cosmochim Acta* 38:1023–1059
  24. Green DH, Hibberson WO, Jaques AL (1979) Petrogenesis of mid-ocean ridge basalts. In: McElhinny MW (ed) *The Earth: its origin, structure and evolution*. Academic Press, London, pp 265–290
  25. Falloon TJ, Green DH, Danushevsky L (2007) Crystallization temperatures of tholeiite parental liquids: implications for the existence of thermally driven mantle plumes. In: Foulger GR, Jurdy DM (eds) *The origins of melting anomalies: plates, plumes, and planetary processes*. Geological Society of America Special Paper 430, Boulder, CO, pp 235–260
  26. Hart SR, Zindler A (1986) In search of a bulk-earth composition. *Chem Geol* 57:247–267
  27. Norman MD, Garcia M (1999) Primitive magmas and source characteristics of the Hawaiian plume: petrology and geochemistry of shield picrites. *Earth Planet Sci Lett* 168:27–44
  28. Ford CE, Russell DG, Craven JA et al (1983) Olivine-liquid equilibria: temperature, pressure and composition dependence of the crystal/liquid cation partition for Mg, Fe<sup>2+</sup>, Ca and Mn. *J Petrol* 24:256–265
  29. Norman MD, Garcia M, Kamenetsky VS et al (2002) Olivine-hosted melt inclusions in Hawaiian picrites: equilibration, melting and plume source characteristics. *Chem Geol* 183:143–168
  30. Stolper EM, Sherman S, Garcia M et al (2004) Glass in the submarine section of the HSDP2 drill core: Hilo, Hawaii. *Geochem Geophys Geosyst* (G3) 5:Q07G15. doi:10.1029/2003GC000553
  31. Green DH, Ringwood AE (1967) The genesis of basaltic magmas. *Contrib Mineral Petrol* 15:103–190
  32. Stolper EM (1980) A phase diagram for mid-ocean ridge basalts: preliminary results and implications for petrogenesis. *Contrib Mineral Petrol* 74:13–27
  33. Eggins SM (1992) Petrogenesis of Hawaiian tholeiites: 1, phase equilibrium constraints. *Contrib Mineral Petrol* 110:387–397
  34. Eggins SM (1992) Petrogenesis of Hawaiian tholeiites: 2, aspects of dynamic melt segregation. *Contrib Mineral Petrol* 110:398–410
  35. Green DH, Falloon TJ (1998) Pyrolite: a ringwood concept and its current expression. In: Jackson INS (ed) *The Earth's mantle: composition, structure and evolution*. Cambridge University Press, Cambridge, pp 311–380
  36. Green DH, Edgar AD, Beasley P et al (1974) Upper mantle source for some hawaiites, mugearites and benmoreites. *Contrib Mineral Petrol* 48:33–43
  37. Irving AJ (1974) Megacrysts from the Newer Basalts and other basaltic rocks from southeastern Australia. *Geol Soc Am Bull* 85:1503–1514
  38. Irving AJ, Price RC (1981) Geochemistry and evolution of lherzolite-bearing phonolitic rocks from Nigeria, Australia, East Germany and New Zealand. *Geochim Cosmochim Acta* 45:1309–1320
  39. Irving AJ, Green DH (2008) Phase relationships of hydrous alkaline magmas at high pressures: production of nepheline hawaiitic–mugearitic liquids by amphibole-dominated fractional crystallization within the lithospheric mantle. *J Petrol* 49:741–756
  40. Green DH, Hibberson WO (1970) Experimental duplication of conditions and precipitation of high pressure phenocrysts in a basaltic magma. *Phys Earth Planet Inter* 3:247–254
  41. Green DH (1973) Conditions of melting of basanite magma from garnet peridotite. *Earth Planet Sci Lett* 17:456–465
  42. Brey GP, Green DH (1975) The role of CO<sub>2</sub> in the genesis of olivine melilitite. *Contrib Mineral Petrol* 49:93–103
  43. Bultitude RJ, Green DH (1971) Experimental study of crystal-liquid relationships at high pressures in olivine nephelinitite and basanite compositions. *J Petrol* 12:121–147
  44. Brey GP, Green DH (1976) Solubility of CO<sub>2</sub> in olivine melilitite at high pressure and role of CO<sub>2</sub> in the Earth's upper mantle. *Contrib Mineral Petrol* 55:217–230
  45. Brey GP, Green DH (1977) Systematic study of liquidus phase relations in olivine melilitite + H<sub>2</sub>O + CO<sub>2</sub> at high pressures and petrogenesis of an olivine melilitite magma. *Contrib Mineral Petrol* 61:141–162
  46. Edgar AD, Green DH, Hibberson WO (1976) Experimental petrology of a highly potassic magma. *J Petrol* 17:339–356
  47. Adam J (1990) The geochemistry and experimental petrology of sodic alkaline basalts from Oatlands, Tasmania. *J Petrol* 31:1201–1223
  48. Ryabchikov IE, Green DH (1978) The role of carbon dioxide in the petrogenesis of highly potassic magmas. In: *Problems of the petrology of the Earth's crust and upper mantle*. Akad. Nauk.

- USSR, Siberian Region, Trudi, Institute of Geology and Geophysics, Novosibirsk, pp 49–64
49. Green DH (1971) Composition of basaltic magmas as indicators of conditions of origin: application to oceanic volcanism. *Philos Trans R Soc Lond A* 268:707–725
  50. Green DH (1972) Magmatic activity as the major process in the chemical evolution of the Earth's crust and mantle. *Tectonophysics* 13:47–71
  51. Green DH, Hibberson WO, Rosenthal A et al (2014) Experimental study of the influence of water on melting and phase assemblages in the upper mantle. *J Petrol* 55:2067–2096
  52. Frey FA, Green DH, Roy SD (1978) Integrated models of basalt petrogenesis—a study of quartz tholeiites to olivine melilitites from southeastern Australia utilizing geochemical and experimental petrological data. *J Petrol* 19:463–513
  53. Katz RF, Spiegelman M, Langmuir CH (2003) A new parameterization of hydrous mantle melting. *Geochem Geophys Geosyst* (G3) 4:1073. doi:[10.1029/2002GC000433](https://doi.org/10.1029/2002GC000433)
  54. Hirschmann MM, Tenner TJ, Aubaud C et al (2009) Dehydration melting of nominally anhydrous mantle: the primacy of partitioning. *Phys Earth Planet Inter* 176:54–68
  55. Grove TL, Chatterjee N, Parman SW et al (2006) The influence of H<sub>2</sub>O on mantle wedge melting. *Earth Planet Sci Lett* 249:74–89
  56. Till CB, Grove TL, Withers AC (2012) The beginnings of hydrous mantle wedge melting. *Contrib Mineral Petrol* 163:669–688
  57. Fumagalli P, Zanchetta S, Poli S (2009) Alkalis in phlogopite and amphibole and their effects on phase relations in metasomatized peridotite: a high pressure study. *Contrib Mineral Petrol* 158:723–737
  58. Kovács I, Green DH, Rosenthal A et al (2012) An experimental study of water in nominally anhydrous minerals in the upper mantle near the water saturated solidus. *J Petrol* 53:2067–2093
  59. Green DH, Hibberson WO, Kovács I et al (2010) Water and its influence on the lithosphere–asthenosphere boundary. *Nature* 467:448–451
  60. Niida K, Green DH (1999) Stability and chemical composition of pargasitic amphibole in MORB pyroxene under upper mantle conditions. *Contrib Mineral Petrol* 135:18–40
  61. Wyllie PJ (1978) Mantle fluid compositions buffered in peridotite–CO<sub>2</sub>–H<sub>2</sub>O by carbonates, amphibole, and phlogopite. *J Geol* 86:687–713
  62. Wyllie PJ (1979) Magmas and volatile components. *Am Mineral* 64:469–500
  63. Eggler DH (1978) The effect of CO<sub>2</sub> upon melting in the system Na<sub>2</sub>O–CaO–Al<sub>2</sub>O<sub>3</sub>–MgO–SiO<sub>2</sub>–CO<sub>2</sub> to 35 kb with an analysis of melting in a peridotite–H<sub>2</sub>O–CO<sub>2</sub> system. *Am J Sci* 278:305–343
  64. Wallace ME, Green DH (1988) An experimental determination of primary carbonatite magma composition. *Nature* 335:343–346
  65. Yaxley GM, Green DH (1996) Experimental reconstruction of sodic dolomitic carbonatite melts from metasomatized lithosphere. *Contrib Mineral Petrol* 124:359–369
  66. Yaxley GM, Crawford AJ, Green DH (1991) Evidence for carbonatite metasomatism in spinel peridotite xenoliths from W. Victoria, Australia. *Earth Planet Sci Lett* 107:305–317
  67. Scott JM, Hodgkinson A, Palin JM et al (2014) Ancient melt depletion overprinted by young carbonatitic metasomatism in the New Zealand lithospheric mantle. *Contrib Mineral Petrol*. doi:[10.1007/s00410-014-0963-0](https://doi.org/10.1007/s00410-014-0963-0)
  68. O'Reilly SY, Griffin WL (1985) A xenoliths-derived geotherm for south-eastern Australia and its geophysical implications. *Tectonophysics* 111:41–63
  69. Nickel KG, Green DH (1984) The nature of the upper-most mantle beneath Victoria, Australia, as deduced from ultramafic xenoliths. In: Kornprobst J (ed) *Kimberlites II: the mantle and crust–mantle relationships*. Elsevier, Amsterdam, pp 161–178
  70. Green DH, Wallace ME (1988) Mantle metasomatism by ephemeral carbonatite melts. *Nature* 336:459–462
  71. Sweeney RJ (1994) Carbonatite melt compositions in the Earth's mantle. *Earth Planet Sci Lett* 128:259–270
  72. Falloon TJ, Green DH (1988) Anhydrous partial melting of peridotite from 8 to 35 kb and the petrogenesis of MORB. *J Petrol* 29:379–414
  73. Green DH (2015) Experimental petrology of peridotites, including effects of water and carbon on melting in the Earth's upper mantle. *Phys Chem Miner* 42:95–102. doi:[10.1007/s00269-014-0729-2](https://doi.org/10.1007/s00269-014-0729-2)
  74. Green DH, Schmidt MW, Hibberson WO (2004) Island arc ankaramites: primitive melts from fluxed refractory lherzolitic mantle. *J Petrol* 45:391–403
  75. Crawford AJ, Falloon TJ, Green DH (1989) Classification, petrogenesis and tectonic setting of boninites. In: Crawford AJ (ed) *Boninites and related rocks*. Unwin Hyman, London, pp 1–49
  76. Faul UH, Jackson INS (2007) Diffusion creep of dry, melt-free olivine. *J Geophys Res* 112:B04204. doi:[10.1029/2006JB004586\(2007\)](https://doi.org/10.1029/2006JB004586(2007))
  77. Eggins SM (1993) Origin and differentiation of picritic arc magmas: Ambae (Aoba), Vanuatu. *Contrib Mineral Petrol* 114:79–100
  78. Faul UH (2001) Melt retention and segregation beneath mid-ocean ridges. *Nature* 410:920–923
  79. Barsdell M, Berry R (1990) The petrology and geochemistry of Western Epi. *J Petrol* 31:747–777
  80. Simon NSC, Neumann ER, Bonadiman C et al (2008) Ultra-refractory domains in the oceanic mantle lithosphere sampled as mantle xenoliths at oceanic islands. *J Petrol* 49:1223–1251
  81. Falloon TJ, Green DH, Danyushevsky LV et al (1999) Peridotite melting at 1 and 1.5 GPa: an experimental evaluation of techniques using diamond aggregates and mineral mixes for determination of near-solidus melts. *J Petrol* 40:1343–1375